EFFICIENCY-OPTIMAL OPERATING CONDITIONS FOR SINGLE-PHASE INDUCTION MOTORS

by

GERALD FLOYD CUMMINGS

B.A.Sc., The University of British Columbia, 1991

A THESIS SUBMITTED IN PARTIAL FULFILLMENT OF

THE REQUIREMENTS FOR THE DEGREE OF

MASTER OF APPLIED SCIENCE

in

THE FACULTY OF GRADUATE STUDIES
(Electrical Engineering)

We accept this thesis as conforming
to the required standard

THE UNIVERSITY OF BRITISH COLUMBIA
April, 1995

In presenting this thesis in partial fulfilment of the requirements for an advanced degree at the University of British Columbia, I agree that the Library shall make it freely available for reference and study. I further agree that permission for extensive copying of this thesis for scholarly purposes may be granted by the head of my department or by his or her representatives. It is understood that copying or publication of this thesis for financial gain shall not be allowed without my written permission.

Department of ELECTRICAL ENGINEERING

The University of British Columbia
Vancouver, Canada

Date 95/04/24

DE-6 (2/88)

Abstract

The double-revolving field model is used to determine theoretically efficiency-optimal operating conditions for single-phase induction motors equipped with an auxiliary winding. The algorithm developed determines the optimal values of main winding current, auxiliary winding current and stator frequency for any desired combination of torque and rotor speed within the motor's ratings. Computer simulations are presented to validate theoretical results and relate optimal terminal voltages to computed winding currents. Experimental measurements made on a 2 pole, 1 hp, 230V submersible motor are compared with computer simulations. These measurements reveal that while it is most important to control core losses by matching the V/Hz ratio to the load, it is possible to make further efficiency improvements by exciting the auxiliary winding.

Contents

List of Tables

List of Figures

Acknowledgments

The author would like to thank Dr. W.G. Dunford of the University of British Columbia Department of Electrical Engineering and Dr. J.B. Neilson of POWERTECH Labs for their financial support, patience, and valued advice. A portion of this work was completed at POWERTECH Labs and the use of facilities there was greatly appreciated.

I am honored to express special thanks to my father who did an excellent job of designing and constructing the test fixture used for experimental measurements.

Others who have been very helpful include Mr. Lloyd Welder, Mr. Alan Prince and Mr. Dave Fletcher at the University of British Columbia Department of Electrical Engineering. While at POWERTECH Labs, Mr. Brian Ferguson, Mr. Jerry Albrecht, Mr. Walter Zarecki and Mr. Peter Wuntschek were valuable sources of advice. Mr. Kenneth George and Mr. Joe Weber of Franklin Electric Corporation were also very helpful in providing motor performance characteristics.

1 Introduction

Single-phase induction motors are commonly used in many applications. A typical home utilizes many fractional horsepower single-phase motors in appliances such as refrigerators, washers and dryers to name only a few. Small single-phase motors are often less expensive to purchase and install than similarly sized three-phase motors and so are often used even where three-phase power is readily available. In rural areas where three-phase power is not usually available, single-phase motors of up to 10 horsepower are in common use.

In general the efficiencies of small single-phase motors are quite low. In the past, motors have been connected directly to the utility line and so have been restricted to operation at fixed voltage and frequency. In the past two decades, considerable attention has been given to efficiency optimization of line operated single-phase induction motors with the most common solution being the placement of a capacitor in series with the auxiliary winding[5, 3]. An alternative arrangement, described by Huang[5], is known as the Wanlass connection and places a capacitor in series with the main winding. Substantial efficiency improvements are reported for both connections and these improvements are primarily attributed to equalization of the current densities in the main and auxiliary windings[5]. Both solutions are limited by the fact that the capacitance required for optimum efficiency is strongly load dependent[3]. In addition, as will be shown, efficiency is

affected by both the magnitude and phase of the auxiliary winding current and so a simple capacitor can not provide the maximum possible efficiency dictated by motor parameters.

As the cost of power electronics continues to decrease, variable voltage variable frequency drives are finding widespread application. As energy costs increase, at some point it may become economical to retrofit existing single-phase motors with such power converters. Although the greatest increase in efficiency would result from applying this technology to both main and auxiliary windings, some improvement could be realized by leaving the main winding directly connected to the utility line and powering the auxiliary winding from a variable voltage power converter. Such a system would operate in much the same way as a capacitor run motor with the advantage that both the magnitude and the phase of the auxiliary winding current could be independently adjusted depending on the load. This approach has been used by Collins[4] to effect a variable speed drive which is claimed to improve efficiency only indirectly. A variation of the approach is proposed by Lettenmaier[7] and although reference is made to possible efficiency improvements, this author's objective is the minimization of pulsating torque.

If variable frequency drives are ever to be applied to single-phase induction motors it will be important to know the optimal operating conditions for the motor. Although there are several papers which report efficiency improvements

by optimization of the run capacitor[3, 5] and operation at reduced V/Hz ratios[6], the author was unable to find any analysis which optimizes efficiency over all degrees of freedom. The theory developed here assumes a linear model and is used to determine the optimal choice of frequency, main and auxiliary winding currents and auxiliary winding phase for any desired operating point. A secondary result is the optimization of starting torque which will be shown to be a special case of efficiency optimization.

Variable frequency drives are in some instances already used in conjunction with single-phase induction motors in remote areas where utility power is not available. Here, one of the most common power sources is solar energy provided by photo-voltaic arrays. As the cost of these solar panels is typically $5 per peak Watt, considerable savings could be realized by optimizing the efficiency of the motors they power and so reducing the size of the array required. Starting performance is also a consideration in these applications and so a system which could also optimize starting torque could provide additional value.

One example of such an installation is the aeration of remote northern lakes. During the winter when these lakes are frozen over they become low in oxygen and as a result some species of fish do not survive. To increase the oxygen levels it is necessary to provide continuous aeration. To this end, a number of installations utilize Air-O-Lator fan type impellers coupled to submersible single-phase induction motors which are powered by photo-voltaic arrays. One motor

commonly used in these installations is a Franklin Electric model 2143084416 which is rated for 1 HP at 3450 RPM. The same motor is used here for experimental work so that the results derived in the remainder of this work might have immediate practical value.

What follows is a theoretical analysis of a single-phase induction motor. The results of this analysis determine operating conditions which theoretically yield the highest possible efficiency. The majority of this analysis is done in closed form but, due to the complexity of the problem, the final step of the optimization is done numerically. To complete the numerical optimization, a knowledge of equivalent circuit parameters is required and these are determined in Appendix A.

Computer simulations are presented in chapter three to demonstrate that the results of the theoretical analysis are correct. Both the theoretical analysis and the corresponding computer simulations assume that the magnitude and phase of the winding currents can be independently and directly controlled. In practice a voltage source is the most cost effective way of supplying power to the windings. A second set of computer simulations is therefore presented to illustrate the effects of changing the magnitude and phase of the winding voltages.

In chapter four experimental results are compared with those predicted by theory and in general there is good agreement. Where there are differences, these can for the most part be attributed to inadequacies in the model used for the analysis. Despite these differences the higher efficiencies predicted by theory are shown to be practically realizable.

2 Theoretical Analysis

2.1 Equivalent Circuit

Two of the most common models used for steady-state analysis of single-phase induction motors are the *Cross-Field*[14, 2, 1] model and the *Revolving-Field*[10, 13, 9, 12, 14] model. The Cross-Field model is based on a D-Q axis representation of the machine while the Revolving-Field model assumes two sinusoidal flux waves rotating in opposite directions. Although both models can easily be extended to include an auxiliary winding, the Revolving-Field model is somewhat more popular and is therefore used as the basis for this work. A paper presented by W.J. Morrill [10] in 1929 is one of the earliest and most complete derivations of the theory. His analysis has since been followed by many authors[13, 9, 12, 14].

The operation of all rotary induction motors depends on the presence of a rotating mmf in the air gap. If there is any differential in speed (slip) between the rotor and this flux wave, the rotor bars cut the lines of flux and emf's are induced in the rotor. The induced emf's generate currents which flow through the rotor impedance. Torque is produced when the flux due to these induced rotor currents interacts with the flux due to the stator windings. In multi-phase motors the necessary rotating mmf is produced by spatial displacement of the stator windings and temporal displacement of the stator currents.

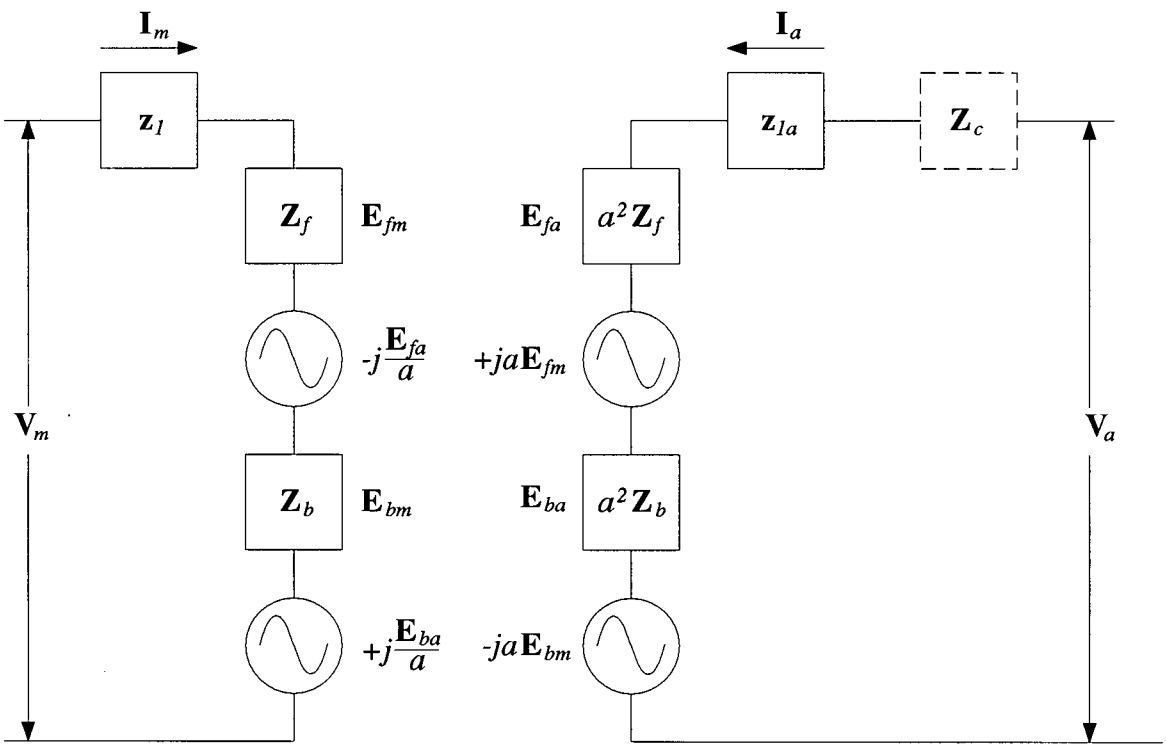

Figure 1: Revolving Field Equivalent Circuit[13]

The mmf produced by the main winding of a single-phase induction motor is stationary and varies sinusoidally with time. Central to the Revolving-Field theory is the fact that such a stationary flux can be resolved into two constant amplitude counter-rotating fluxes, each with half the amplitude of the stationary flux. Provided the rotor is stationary, the currents induced in the rotor bars by these fluxes are equal and opposite and consequently no torque is produced. However, if the rotor turns in either direction, the induced emf's are of different frequencies. As a result the rotor impedances are different as are the amplitudes of the induced currents.

The model shown in figure 1 is derived by Cyril G. Veinott in his book Theory and Design of Small Induction Motors[13] and except for differences in nomenclature is the same as Morrill's model. This model describes a single-phase induction motor with a main and auxiliary winding assumed to be in space quadrature. The parameters used in the model and throughout the rest of this work are defined in table 1. All rotor quantities shown are referred to the main winding.

The apparent rotor impedances to forward and backward rotating mmf's, as listed in table 1, are defined by Veinott[13] as:

$$\begin{aligned} R_f &= \frac{x_m}{2}\frac{x_m[r_2/s]}{[r_2/s]^2+[x_m+x_1]^2} \\ X_f &= \frac{x_m}{2}\frac{[r_2/s]^2+x_2[x_m+x_1]}{[r_2/s]^2+[x_m+x_1]^2} \\ R_b &= \frac{x_m}{2}\frac{x_m[r_2/(2-s)]}{[r_2/(2-s)]^2+[x_m+x_1]^2} \\ X_b &= \frac{x_m}{2}\frac{[r_2/(2-s)]^2+x_2[x_m+x_1]}{[r_2/(2-s)]^2+[x_m+x_1]^2} \end{aligned} \tag{1}$$

The left half of the circuit of figure 1 represents the main winding and the right half represents the auxiliary winding. The blocks in the horizontal branches represent stator impedances including an optional run or start capacitor in series with the auxiliary winding. Blocks in the vertical branches model the rotor impedance to forward and backward mmf's. These rotor impedances are referred to the main winding and so terms which appear in the auxiliary winding branch are scaled by a^2 to account for the turns ratio.

a	Auxiliary/Main Turns Ratio	*p.u.*
$\mathbf{E}_{ba}$= $\mathrm{a}^2\mathbf{Z}_b\mathbf{I}_a$	Backward Auxiliary EMF	*V*
$\mathbf{E}_{bm}$= $\mathbf{Z}_b\mathbf{I}_m$	Backward Main EMF	*V*
$\mathbf{E}_{fa}$=$\mathrm{a}^2\mathbf{Z}_f\mathbf{I}_a$	Forward Auxiliary EMF	*V*
$\mathbf{E}_{fm}$=$\mathbf{Z}_f\mathbf{I}_m$	Forward Main EMF	*V*
$\mathbf{I}_a$	Auxiliary Current	*A*
$\mathbf{I}_m$	Main Current	*A*
r_1	Main Stator Resistance	Ω
r_{1a}	Auxiliary Stator Resistance	Ω
r_2	Rotor Resistance	Ω
s	Rotor Slip Frequency	*p.u.*
$\mathbf{V}_a$	Auxiliary Voltage	*V*
$\mathbf{V}_m$	Main Voltage	*V*
x_1	Main Stator Leakage Reactance	Ω
x_{1a}	Auxiliary Stator Leakage Reactance	Ω
x_2	Rotor Leakage Reactance	Ω
x_m	Magnetizing Reactance	Ω
$\mathbf{z}_1$= r_1+jx_1	Main Stator Impedance	Ω
$\mathbf{z}_{1a}$= r_{1a}+jx_{1a}	Auxiliary Rotor Impedance	Ω
$\mathbf{Z}_b$= R_b+jX_b	Apparent Backward Rotor Impedance	Ω
$\mathbf{Z}_c = R_c + jX_c$	Run/Start Capacitor Impedance	Ω
$\mathbf{Z}_f$= R_f+jX_f	Apparent Forward Rotor Impedance	Ω
$\phi = \angle\mathbf{I}_a - \angle\mathbf{I}_m$	Auxiliary Relative Phase	*rad*
ω_m	Rotor Speed	*rad/s*
ω_s	Synchronous Frequency	*rad/s*

Table 1: Equivalent Circuit Symbols

Voltage sources shown in the vertical branches model transformer action

between the main and auxiliary windings. To understand the nature of this coupling it is important to remember that the main and auxiliary windings independently produce both forward and backward rotating mmf's all of which have a constant amplitude. To simplify the discussion, consider the forward rotating mmf produced by the main winding current. This mmf produces a back emf which appears in series with the main winding. Because this back emf is proportional to the main winding current it is most conveniently represented as an impedance $\mathbf{Z}_f = \mathbf{E}_{fm}/\mathbf{I}_m$.

The same mmf also produces a back emf which appears in series with the auxiliary winding and is given by $+ja\mathbf{E}_{fm}$. As in the case of the main winding, peak voltages are induced when the rotating mmf is aligned with the axis of the winding. Because the auxiliary winding is in electrical space-quadrature with respect to the main winding, the peak voltages induced in the auxiliary winding precede those induced in the main winding by one quarter cycle. Consequently, this emf is modelled as a voltage source proportional to the back emf induced in the main winding but phase shifted by one quarter cycle. Because the auxiliary winding does not have the same number of turns as does the main winding, the magnitude of the emf induced in the auxiliary winding is scaled by the turns ratio.

2.2 Performance Calculations

2.2.1 Impedance Matrix

An impedance matrix is easily derived by applying Kirchoff's voltage law to the circuit of figure 1. The equations defining this model can be written as:

$$\begin{aligned} \mathbf{V}_m &= \left[\mathbf{z}_1 + \mathbf{Z}_f + \mathbf{Z}_b\right]\mathbf{I}_m - j\frac{\mathbf{E}_{fa}}{a} + j\frac{\mathbf{E}_{ba}}{a} \\ \mathbf{V}_a &= \left[\mathbf{Z}_c + \mathbf{z}_{1a} + a^2\left(\mathbf{Z}_f + \mathbf{Z}_b\right)\right]\mathbf{I}_a + ja\mathbf{E}_{fm} - ja\mathbf{E}_{bm} \end{aligned} \tag{2}$$

The impedance matrix is obtained by substitution of the four back emf's defined in table 1 and is the same as derived by Matsch[9].

$$\begin{bmatrix} \mathbf{V}_m \\ \mathbf{V}_a \end{bmatrix} = \begin{bmatrix} \mathbf{z}_1 + \mathbf{Z}_f + \mathbf{Z}_b & -ja\left(\mathbf{Z}_f - \mathbf{Z}_b\right) \\ ja\left(\mathbf{Z}_f - \mathbf{Z}_b\right) & \mathbf{Z}_c + \mathbf{z}_{1a} + a^2\left(\mathbf{Z}_f + \mathbf{Z}_b\right) \end{bmatrix} \begin{bmatrix} \mathbf{I}_m \\ \mathbf{I}_a \end{bmatrix} \tag{3}$$

2.2.2 Input Power

The input power is calculated as $P_e = \Re\{\mathbf{V}_m\mathbf{I}_m^* + \mathbf{V}_a\mathbf{I}_a^*\}$. After substitution of the terminal voltages from the impedance matrix this equation can be written as:

$$\begin{aligned} P_e =& \Re\left\{\left[\left(\mathbf{z}_1 + \mathbf{Z}_f + \mathbf{Z}_b\right)\mathbf{I}_m - ja\left(\mathbf{Z}_f - \mathbf{Z}_b\right)\mathbf{I}_a\right]\mathbf{I}_m^*\right\} + \\ & \Re\left\{\left[ja\left(\mathbf{Z}_f - \mathbf{Z}_b\right)\mathbf{I}_m + \left(\mathbf{Z}_c + \mathbf{z}_{1a} + a^2\left(\mathbf{Z}_f + \mathbf{Z}_b\right)\right)\mathbf{I}_a\right]\mathbf{I}_a^*\right\} \end{aligned} \tag{4}$$

Recognizing that $\mathbf{I}_m\mathbf{I}_m^*$ and $\mathbf{I}_a\mathbf{I}_a^*$ are both real, this equation simplifies to:

$$\begin{aligned} P_e =& \left[r_1 + R_f + R_b\right]I_m^2 + \left[R_c + r_{1a} + a^2\left(R_f + R_b\right)\right]I_a^2 \\ & + \Re\left\{ja\left(\mathbf{Z}_f - \mathbf{Z}_b\right)\left[\mathbf{I}_m\mathbf{I}_a^* - \mathbf{I}_a\mathbf{I}_m^*\right]\right\} \end{aligned} \tag{5}$$

Since $\mathbf{I}_m\mathbf{I}_a^* - \mathbf{I}_a\mathbf{I}_m^* = \mathbf{I}_m\mathbf{I}_a^* - (\mathbf{I}_m\mathbf{I}_a^*)^* = -j2I_mI_a\sin\phi$ and R_f and R_b are the real parts of Z_f and Z_b, equation 5 can be reduced to:

$$\begin{aligned} P_e =& \left[r_1 + R_f + R_b\right] I_m^2 + \left[R_c + r_{1a} + a^2\left(R_f + R_b\right)\right] I_a^2 \\ &+ 2aI_mI_a\left(R_f - R_b\right)\sin\phi \end{aligned} \tag{6}$$

where ϕ is the phase of the auxiliary winding current measured with respect to the main winding current.

2.2.3 Output Power and Torque

The torque produced by the machine can be determined by examining the net power transferred across the air gap. The forward rotating mmf's contribute to a positive torque while the backward rotating mmf's contribute to a negative torque. The difference between the forward and backward emf's therefore determines the net power. P_{gm} and P_{ga} are defined here as the air gap power produced by the main and auxiliary windings and can be written as:

$$\begin{aligned} P_{gm} &= \Re\left\{\left[\left(\mathbf{E}_{fm} - j\mathbf{E}_{fa}/a\right) - \left(\mathbf{E}_{bm} + j\mathbf{E}_{ba}/a\right)\right]\mathbf{I}_m^*\right\} \\ P_{ga} &= \Re\left\{\left[\left(\mathbf{E}_{fa} - ja\mathbf{E}_{fm}\right) - \left(\mathbf{E}_{ba} + ja\mathbf{E}_{ba}\right)\right]\mathbf{I}_a^*\right\} \end{aligned} \tag{7}$$

Substituting the back emf equations from table 1 yields:

$$\begin{aligned} P_g &= P_{gm} + P_{ga} \\ &= \Re\left\{\left(\mathbf{Z}_f - \mathbf{Z}_b\right)\left(I_m^2 + a^2I_a^2\right) + ja\left(\mathbf{Z}_f + \mathbf{Z}_b\right)\left(\mathbf{I}_m\mathbf{I}_a^* - \mathbf{I}_a\mathbf{I}_m^*\right)\right\} \end{aligned} \tag{8}$$

After simplification the air gap power can be written as:

$$P_g = \left(R_f - R_b\right)\left(I_m^2 + a^2I_a^2\right) + 2aI_mI_a\left(R_f + R_b\right)\sin\phi \tag{9}$$

This equation is derived in slightly different ways by other authors[13, 9]. The air gap power is given in *synchronous Watts*[10] and so must be multiplied by the per unit rotor speed to compute the total mechanical power. Mechanical output power is given by the difference between total mechanical power and friction and windage losses and can therefore be written as:

$$P_m = (1 - s)P_g - P_{fw} \tag{10}$$

Average torque[13, 9] is computed by dividing the mechanical power by the rotor frequency of $\omega_m = (1 - s)\omega_s$.

$$T = \frac{P_m}{\omega_m} = \frac{(1 - s)P_g - P_{fw}}{(1 - s)\omega_s} = \frac{P_g - P_{fw}}{\omega_s} \tag{11}$$

2.3 Efficiency

The efficiency, can be written as:

$$\eta = \frac{P_m}{P_e} = \frac{(1 - s)P_g - P_{fw}}{(1 - s)P_g + P_d} \tag{12}$$

where P_d represents the electrical losses within the machine.

By inspection of equation 12 it is obvious that efficiency is affected by friction and windage losses as well as electrical losses. Because friction and windage losses depend only upon the operating point, assuming constant slip the only term which affects efficiency at a given operating point is electrical losses. It is therefore of interest to segregate the electrical losses which are distributed between

the rotor and stator. These losses are given by the difference between electrical power and total mechanical power:

$$P_d = P_e - (1-s)P_g = P_e - P_g + sP_g \tag{13}$$

After the appropriate substitutions are made this equation can be written as:

$$\begin{aligned} P_d =& \left[r_1 + sR_f + (2-s)R_b\right] I_m^2 \\ &+ \left[R_c + r_{1a} + a^2\left[sR_f + (2-s)R_b\right]\right] I_a^2 \\ &+ 2a\left[sR_f - (2-s)R_b\right] I_m I_a \sin\phi \end{aligned} \tag{14}$$

A more intuitive understanding can be obtained if the equation is rewritten as:

$$\begin{aligned} P_d =& r_1 I_m^2 + (R_c + r_{1a}) I_a^2 \\ &+ s\left[(R_f - R_b)(I_m^2 + a^2 I_a^2) + 2aI_m I_a (R_f + R_b)\sin\phi\right] \\ &+ 2R_b\left[I_m^2 + a^2 I_a^2 - 2aI_m I_a \sin\phi\right] \end{aligned} \tag{15}$$

In this form, the first term represents stator losses. The second term, which is the product of slip and air-gap power, represents slip dependant rotor losses which are inherent to induction machines. The third term represents additional rotor losses which are due entirely to the asymmetry of the rotating mmf in the air gap. This term can be shown to be zero if and only if $I_m = aI_a$ and $\phi = \pi/2$ in which case the air-gap mmf is symmetrical and the machine is said to be *balanced.* This condition also eliminates pulsating torque: a result derived by a number of authors[7, 4].

2.4 Optimization of Running Performance

Steady-state efficiency is optimized under the assumption that a particular operating point is desired. The operating point is defined by specifying both torque and rotor speed. The controllable variables which affect efficiency are phase of the auxiliary winding current relative to the main winding, the magnitudes of main and auxiliary winding currents, and the stator frequency. Because many terms in equations 6 and 10 are complicated functions of slip, a direct solution seems intractable. To simplify the problem, optimization is done in two stages: an analytical solution which determines main and auxiliary winding currents and their relative phase at an arbitrary stator frequency, followed by a numerical solution which yields the optimum stator frequency. Because the rotor speed is specified by the operating point, if the analytical solution is done assuming constant stator frequency, the slip is constant since $s = (\omega_s - \omega_m)/\omega_s$.

The problem described above is a constrained optimization and so is solved by means of Lagrange multipliers[8]. The objective is to minimize input power with a constraint of constant mechanical power. The solution which gives the optimal efficiency is therefore constrained to the surface defined by equation 10 which must be solved simultaneously with:

$$\begin{aligned} \nabla P_e(I_m, I_a, \phi) &= \tilde{\lambda}(1-s)\nabla P_m(I_m, I_a, \phi) \\ &= \tilde{\lambda}(1-s)\nabla\left[P_g(I_m, I_a, \phi) - P_{fw}\right] \end{aligned} \tag{16}$$

Since P_{fw} is independent of all electrical quantities, and slip is assumed constant, the relationship can be reduced to:

$$\nabla P_e(I_m, I_a, \phi) = \lambda \nabla P_g(I_m, I_a, \phi) \tag{17}$$

where $\lambda = \tilde{\lambda}(1-s)$. In total there are four equations which must be solved simultaneously. The variables in the optimization constitute the first three degrees of freedom and the fourth is the Lagrange multiplier λ.

$$\frac{\partial P_e}{\partial \phi} = \lambda \frac{\partial P_g}{\partial \phi} \tag{18}$$

$$\frac{\partial P_e}{\partial I_m} = \lambda \frac{\partial P_g}{\partial I_m} \tag{19}$$

$$\frac{\partial P_e}{\partial I_a} = \lambda \frac{\partial P_g}{\partial I_a} \tag{20}$$

$$(1-s)P_g = T\omega_m + P_{fw} \tag{21}$$

2.4.1 Auxiliary Winding Current Phase

Equation 18, after substitution and simplification, can be written as:

$$\big(R_f - R_b\big) I_m I_a \cos\phi = \lambda \big(R_f + R_b\big) I_m I_a \cos\phi \tag{22}$$

One solution to this equation is given by:

$$\lambda = \frac{R_f - R_b}{R_f + R_b} \tag{23}$$

Two other solutions are possible when $I_m = 0$ or $I_a = 0$. However, it is easily shown that if any of these three solutions are used, there are no valid solutions

for equations 19 and 20. The only valid solution for equation 22 is therefore given by $\cos\phi = 0$. This equation has roots at $\phi = \pm\pi/2$ and the condition which optimizes efficiency is given by $\phi = \pi/2$. This is justified by careful examination of the air-gap power and power dissipation, as given by equations 9 and 14 respectively.

By inspection, the air-gap power is maximized with respect to ϕ when $\phi = \pi/2$. The same condition minimizes power dissipation and so optimizes efficiency. To prove minimum power dissipation, it is necessary to find the sign of $sR_f - (2-s)R_b$. This term pre-multiplies $sin\phi$ in equation 14 and can be expanded to:

$$\mathrm{sgn}\left\{ \frac{\mathrm{s}\frac{\mathrm{x_m^2}}{2}[\mathrm{r_2/s}]}{[\mathrm{r_2/s}]^2+[x_m+x_1]^2} - \frac{(2-\mathrm{s})\frac{\mathrm{x_m^2}}{2}[\mathrm{r_2}/(2-\mathrm{s})]}{[\mathrm{r_2}/(2-\mathrm{s})]^2+[x_m+x_1]^2} \right\} \tag{24}$$

For $0 \leq s \leq 1$, all quantities in the above equation are positive and the expression is easily reduced to:

$$\mathrm{sgn}\{sR_f - (2-s)R_b\} = \mathrm{sgn}\left\{s^2 - (2-s)^2\right\} = -1 \tag{25}$$

Consequently, $sin\phi$ must be positive to achieve minimum power dissipation and so efficiency is optimized with respect to phase when:

$$\phi = \pi/2 \tag{26}$$

2.4.2 Auxiliary Winding Current Magnitude

To find the simultaneous solution of equations 19 and 20 it is necessary to eliminate the Lagrange multiplier, λ. These equations are easily manipulated to yield:

$$\lambda = \frac{\partial P_e}{\partial I_m} / \frac{\partial P_g}{\partial I_m} = \frac{\partial P_e}{\partial I_a} / \frac{\partial P_g}{\partial I_a} \tag{27}$$

The optimal auxiliary winding current can now be determined as a ratio of the required main winding current. Defining this ratio as $k = I_a/I_m$ and letting $\phi = \pi/2$, the above equation becomes:

$$\begin{aligned} &\frac{(r_1 + R_f + R_b) + a(R_f - R_b)k}{(R_f - R_b) + a(R_f + R_b)k} \\ &= \frac{[R_c + r_{1a} + a^2(R_f + R_b)]k + a(R_f - R_b)}{a^2(R_f - R_b)k + a(R_f + R_b)} \end{aligned} \tag{28}$$

After cross-multiplication and simplification this equation can be written in quadratic form:

$$\begin{aligned} &\left[4a^3 \frac{R_f R_b}{R_f + R_b} + a(R_c + r_{1a})\right] k^2 \\ &+ \left[\frac{R_f - R_b}{R_f + R_b}(R_c + r_{1a} - a^2 r_1)\right] k \\ &- \left[4a \frac{R_f R_b}{R_f + R_b} + a r_1\right] = 0 \end{aligned} \tag{29}$$

If stator losses are assumed to be zero, this equation reduces to $a^2k^2 = 1$ which implies that $I_m = aI_a$ and, as noted previously, the machine is balanced. When stator losses can not be neglected the optimal value for k is given by:

$$k = \frac{-B \pm \sqrt{B^2 - 4AC}}{2A} \tag{30}$$

where:

$$A = 4a^3\frac{R_f R_b}{R_f + R_b} + a(R_c + r_{1a})$$
$$B = \frac{R_f - R_b}{R_f + R_b}(R_c + r_{1a} - a^2 r_1) \tag{31}$$
$$C = -4a\frac{R_f R_b}{R_f + R_b} - ar_1$$

Because k is defined as the ratio of the magnitude of two vector quantities, only positive values are allowed. By inspection, for $0 \leq s \leq 1$, A is positive and C is negative so $-4AC > 0$ and $\sqrt{B^2 - 4AC} > |B|$. The optimal choice for k is therefore given by

$$k = \frac{-B + \sqrt{B^2 - 4AC}}{2A} \tag{32}$$

2.4.3 Main Winding Current Magnitude

It now remains to satisfy the constraint given by equation 21. With $\phi = \pi/2$, this relationship can be written as:

$$(R_f - R_b)(I_m^2 + a^2 I_a^2) + 2a(R_f + R_b)I_m I_a = \frac{T\omega_m + P_{fw}}{1 - s} \tag{33}$$

After substitution of the previously computed value for k the solution is:

$$I_m = \sqrt{\frac{T\omega_m + P_{fw}}{(1 - s)\left[(1 + a^2k^2)(R_f - R_b) + 2ak(R_f + R_b)\right]}} \tag{34}$$

2.4.4 Stator Frequency

The final step in the optimization is to determine the optimal stator frequency. Equations 26, 32, and 34 define the optimal main and auxiliary winding currents

assuming fixed output power and a constant stator frequency. Because the above relationships are strongly dependent on slip, an analytical solution for the optimal stator frequency is intractable and a numerical solution is the only remaining option. Such an optimization requires knowledge of the equivalent circuit parameters and an experimental determination of these parameters, is presented in Appendix A. These parameters are used throughout the remainder of this work.

2.5 Optimization of Starting Performance

Starting performance is optimized by assuming that a known value of starting torque is required. The objective is therefore to minimize the input power required to achieve this value of torque. The analysis given in the preceding section optimizes efficiency by minimizing losses with a constraint of constant mechanical power. Because slip is assumed constant throughout the analysis this constraint is equivalent to one of constant air-gap power. Torque and air-gap power are related by equation 11 and so the optimal starting conditions are only a special case of the solution to equations 18 through 21.

The optimal phase angle between main and auxiliary winding currents is therefore as before:

$$\phi = \pi/2 \tag{35}$$

At standstill $s = 1$ and the forward and backward rotor resistances of equation 1 reduce to:

$$R_f = R_b = \frac{x_m}{2} \frac{x_m r_2}{r_2^2 + (x_m + x_1)^2} \tag{36}$$

The optimal ratio of magnitudes between main and auxiliary winding currents, as defined by equation 32, can therefore be reduced to:

$$k = \sqrt{\frac{x_m^2 r_2 + r_1 \left[r_2^2 + (x_m + x_1)^2 \right]}{a^2 x_m^2 r_2 + (R_c + r_{1a}) \left[r_2^2 + (x_m + x_1)^2 \right]}} \tag{37}$$

The required main winding current is given by:

$$I_m = \sqrt{\frac{\left[r_2^2 + (x_m + x_1)^2 \right] T \omega_s}{2ak x_m^2 r_2}} \tag{38}$$

3 Simulation Results

Computer simulations are provided to validate theoretical results as well as to predict optimal operating conditions for specified load conditions. The equations describing the model were implemented in Matlab® using the parameters derived in Appendix A. It is assumed throughout these simulations that the motor is supplied by a variable frequency drive and that there is no limitation on stator frequency.

3.1 Validation of Theoretical Results

Theory predicts that, given any load condition, efficiency can be maximized by proper choice of auxiliary winding current (both magnitude and phase) and stator frequency. These results are verified by computing the optimal operating conditions at rated speed and for several values of torque. Efficiency is plotted as each of these three parameters are varied about their optimal values.

The first result predicted by theory is that efficiency is maximized when the auxiliary winding current leads the main winding current by 90°. Figure 2 shows a plot of efficiency vs. auxiliary winding phase and it is apparent that, as predicted, efficiency is maximized when the auxiliary and main winding currents are in quadrature.

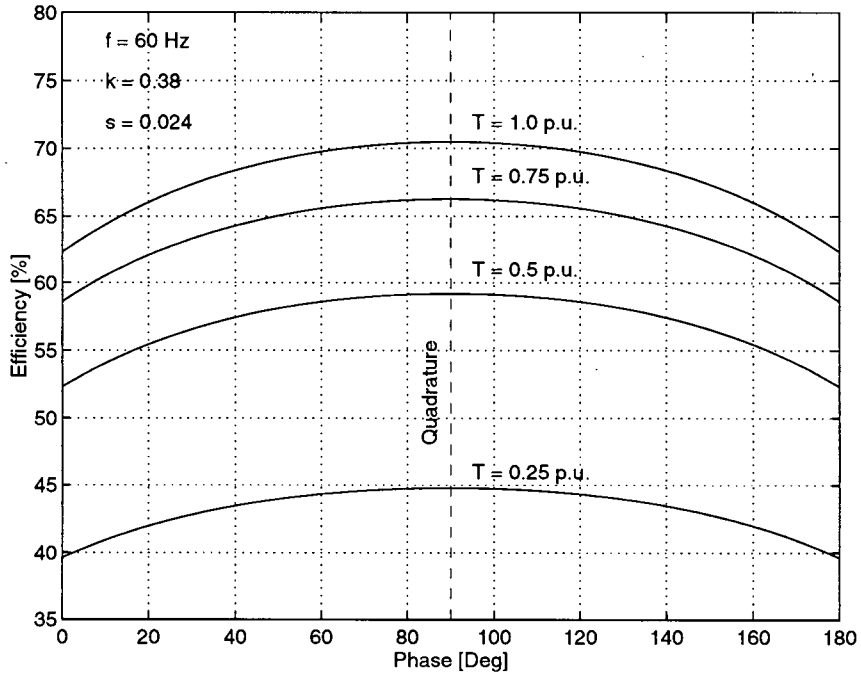

Figure 2: Efficiency vs. Auxiliary Current Phase Angle

Peak efficiency is predicted when the magnitude of the auxiliary winding current is in fixed proportion to that of the main winding. This constant of proportionality can be computed from equation 32 and at rated speed the optimal value is $k = 0.38$. Figure 3 plots efficiency against the auxiliary winding current in per unit of main winding current illustrating that peak efficiency is obtained at the predicted value.

The final variable in the optimization is slip. Because the rotor speed is fixed the optimal value of slip determines the optimum stator frequency. Because of the complicated relationship between slip and efficiency, an analytic solution could not be obtained and so there is no numerical value to be compared with the

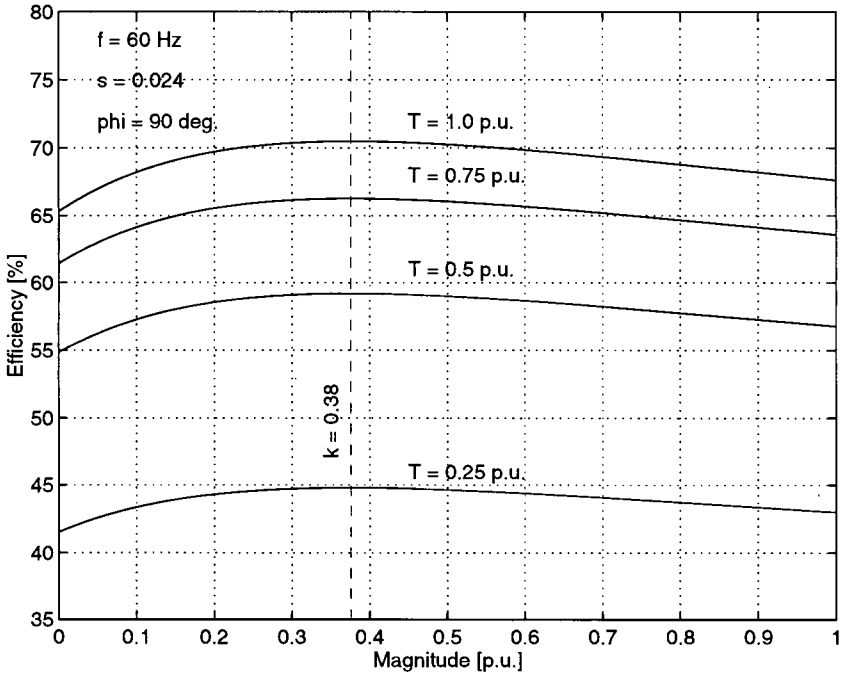

Figure 3: Efficiency vs. Auxiliary Current Magnitude

results shown in figure 4. A numerical optimization indicates that peak efficiency is obtained when $s = 0.024$. Computer simulations reveal that the optimal slip depends only on rotor speed and is independent of torque. The same is true of auxiliary winding current magnitude and this can be seen by examination of equation 32.

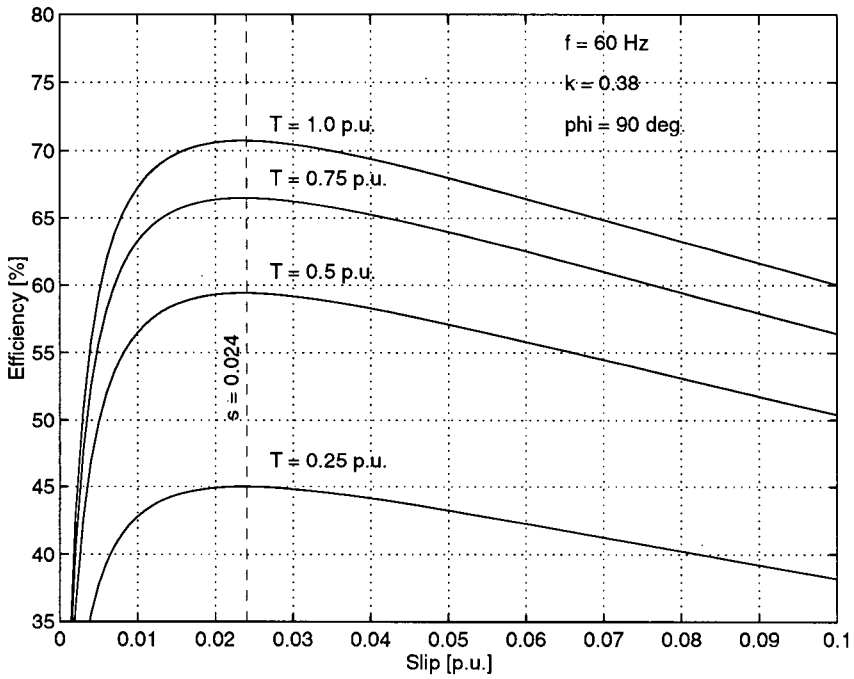

Figure 4: Efficiency vs. Slip

3.2 Optimal Winding Currents

As noted in the previous section, when properly normalized, optimal operating conditions depend only on rotor speed and are independent of torque. The following figures plot these optimal conditions against rotor speed. It should be noted that because slip is one of the variables in the optimization, stator frequency is not constant and is determined by the rotor speed and the optimum slip.

Figure 5 plots the optimum auxiliary winding current as a fraction of the main winding current. Note that this ratio is relatively constant for practical values of

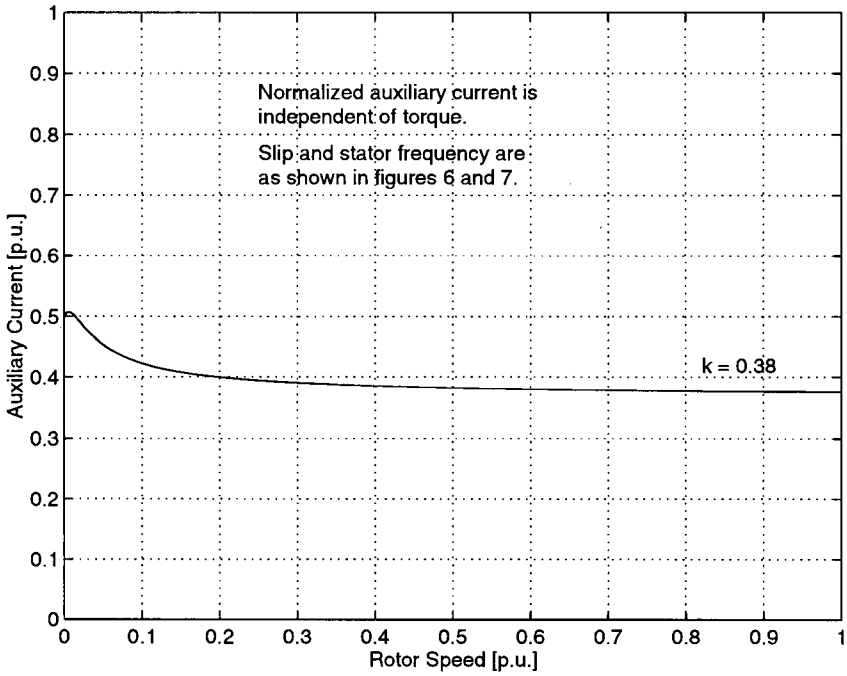

Figure 5: Optimal Auxiliary Current Magnitude vs. Rotor Speed

rotor speed and that at rated speed $k = 0.38$. This value is consistent with that shown in figure 3.

The slip which provides the highest efficiency, as determined by numerical optimization, is plotted against rotor speed in figure 6. At rated speed the optimal slip is $s = 0.024$ as is also shown in figure 4. Stator frequency can be computed from the optimum slip and is plotted against rotor speed in figure 7. Very little error is introduced by linearizing this relationship and the least-squares fit is given by $\omega_s \approx \omega_m + 0.026$.

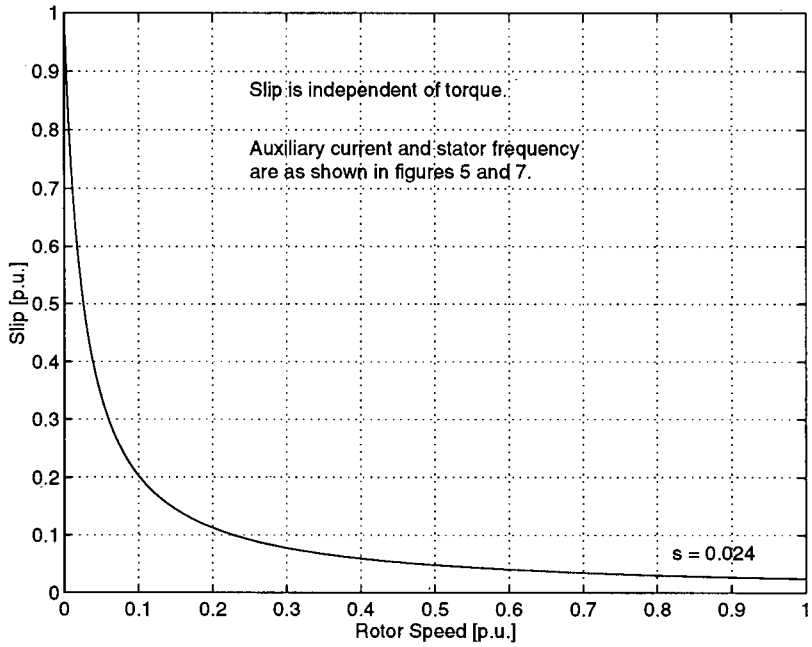

Figure 6: Optimal Slip vs. Rotor Speed

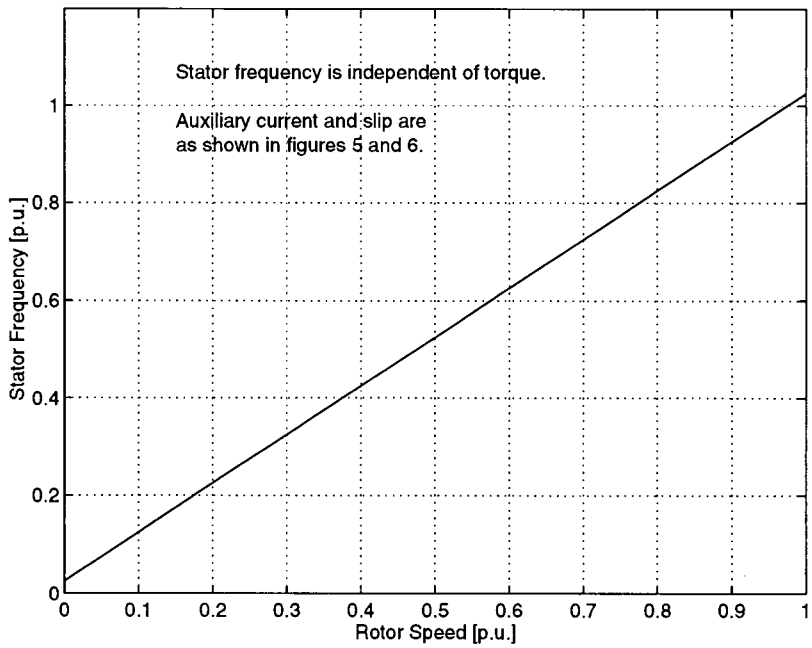

Figure 7: Optimal Stator Frequency vs. Rotor Speed

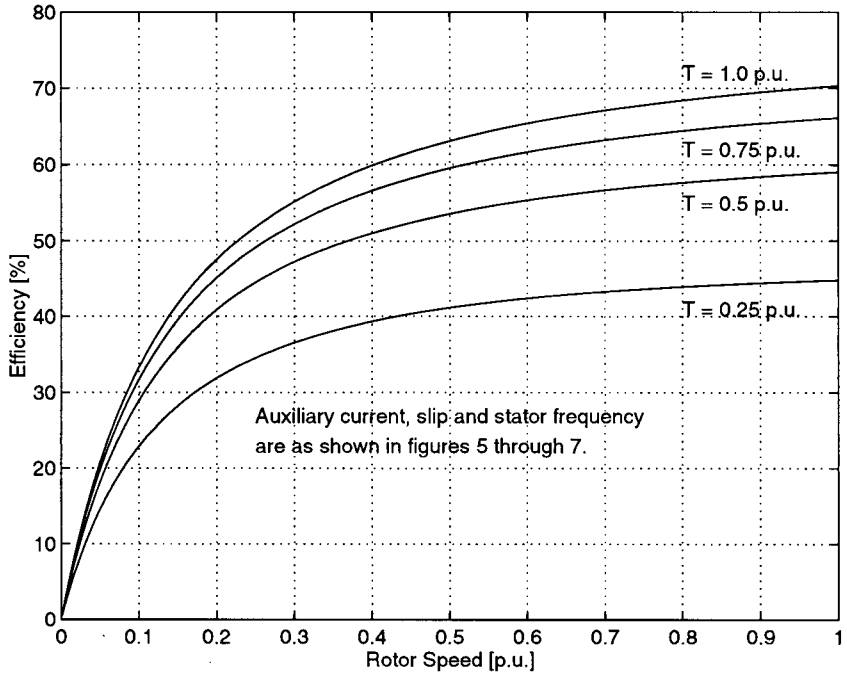

Figure 8: Maximum Efficiency vs. Rotor Speed

Although the optimal operating conditions are independent of torque, the maximum efficiency is related to torque. Under no-load conditions, the total torque produced by the motor is exactly equal to friction and windage torque. Conversely, when the motor is heavily loaded, friction and windage torque is only a small fraction of the total torque produced. Consequently, efficiency increases with load torque until electrical losses become dominant. The maximum efficiencies for selected values of load torque are plotted against rotor speed in figure 8.

3.3 Optimal Winding Voltages

Terminal voltages can be determined by applying the impedance matrix of equation 3 to the results derived in the preceding section. Main winding voltage is plotted against mechanical speed in figure 9.

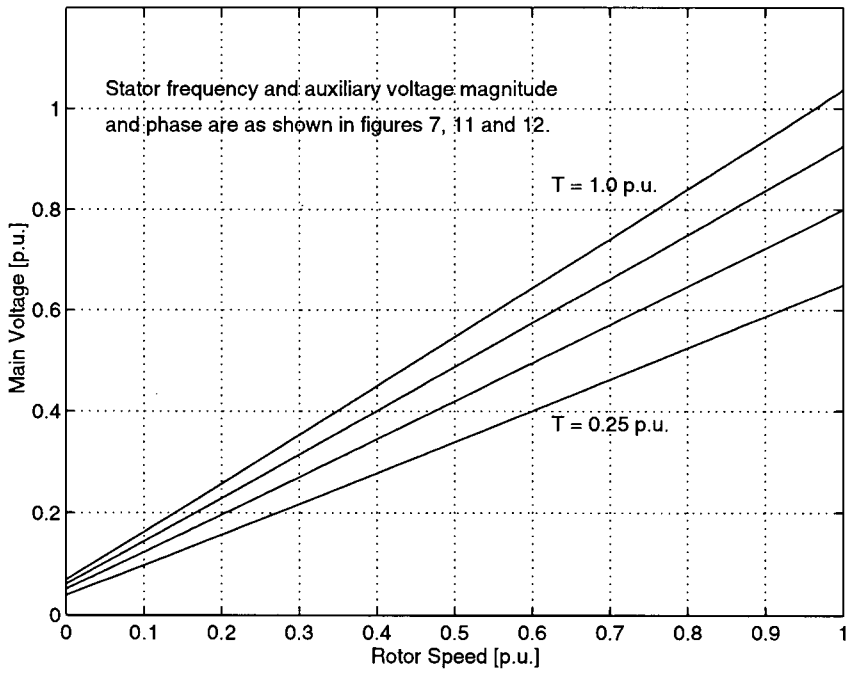

Figure 9: Optimal Main Voltage Magnitude vs. Rotor Speed

The V/Hz ratio can be computed from the main winding voltage and the optimal stator frequency determined in the previous section. These results are plotted in per unit of rated V/Hz against rotor speed in figure 10. The optimal V/Hz ratio increases very sharply at low speeds in order to compensate for the

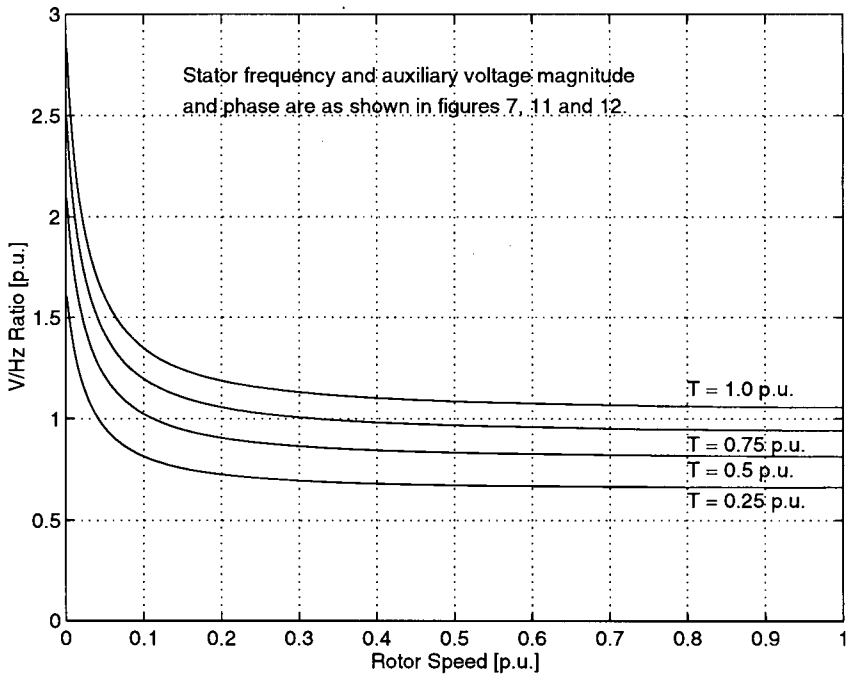

Figure 10: Optimal Main V/Hz Ratio vs. Rotor Speed

proportionally higher voltage drop across the stator resistance. This low-frequency voltage boost is a common feature of commercially available drive systems[11].

At near rated speed and torque, because a linear model has been assumed the optimal per unit V/Hz ratio predicted by theory exceeds unity. In practice, operating under these conditions would result in saturation of the magnetic circuit and the efficiency would be much lower than predicted. The practical significance of this figure is therefore that the V/Hz ratio should be reduced when the machine is operated under light load conditions. When increased torque is desired, the V/Hz ratio should be increased but should only exceed its rated value at very low speed.

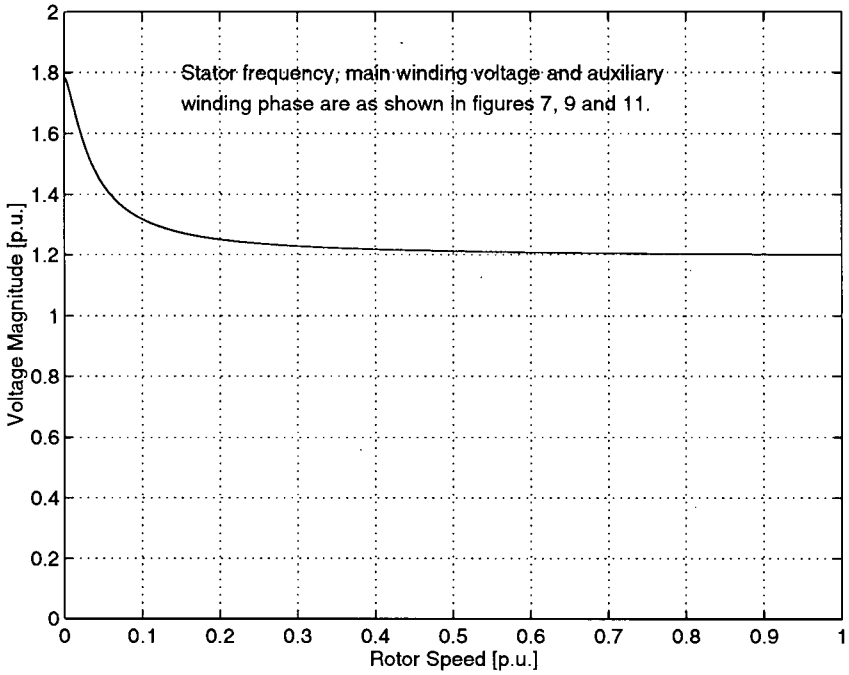

Figure 11: Optimal Auxiliary Voltage Magnitude vs. Rotor Speed

The optimal auxiliary winding voltage is plotted as a fraction of the optimal main winding voltage in figure 11 and it is apparent that this ratio is nearly constant for practical values of rotor speed. Figure 12 plots the relative phase of the auxiliary winding voltage against mechanical speed. Again, for practical values of mechanical speed, the phase is nearly constant.

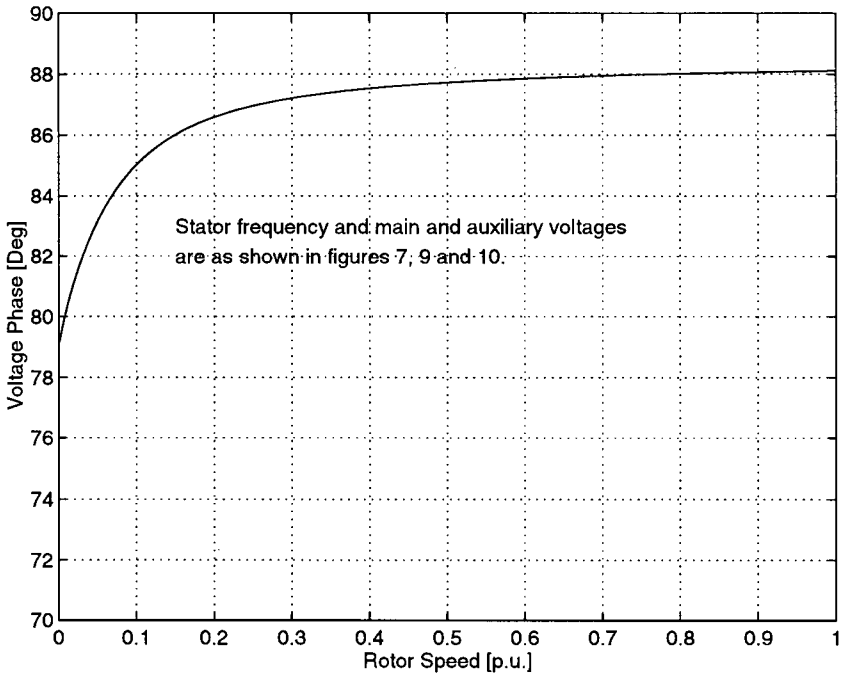

Figure 12: Optimal Auxiliary Voltage Phase Angle vs. Rotor Speed

4 Experimental Results

4.1 Apparatus

4.1.1 Motor

Experimental measurements were made on a Franklin Electric model 2143084416 submersible motor rated for 1 HP at 3450 RPM. This rating is given assuming that the motor is immersed in water and is therefore adequately cooled. For the purposes of experimental work this cooling requirement was met by mounting the motor in a drum filled with water.

4.1.2 Load

A heavy duty 24V automotive alternator was directly coupled to the motor under test. The alternator was prepared by machining shoulders on the end bells. These shoulders were concentric with the alternator shaft and were designed to accept bearings. With this arrangement, when mounted in the test fixture, both the alternator shaft and housing were free to rotate.

Torque sensing was accomplished by locating a load cell between the alternator housing and a stationary part of the test fixture, preventing rotation of the alternator housing. The load cell output was therefore proportional to the total torque produced by the motor under test. A fitting was located on the alternator housing to accept a torque wrench for the purpose of calibrating the load cell.

The rectifiers were removed from the alternator and its windings were short-circuited. With this connection the total power generated by the alternator was dissipated by the alternator windings. An external resistive load bank would have been preferable as it would have reduced heating in the alternator but the resistance required to achieve a reasonable power transfer was too low to be practical. By applying a field current of approximately 2A the alternator produced a braking torque equal to the rated torque of the motor under test.

4.1.3 Supply

All of the measurements reported here were made at line frequency and with a 208V three phase supply. Variacs were used to adjust the magnitudes of the main and auxiliary winding voltages and an adjustable phase shifting transformer was used for variable phase measurements. The majority of tests were run with a fixed phase of approximately 90° between the main and auxiliary winding voltages. This phase shift was accomplished by Scott-connected isolation transformers.

4.1.4 Instrumentation

All electrical quantities were measured using a Data Precision model Data 6000A waveform analyzer. Isolation amplifiers were used to interface the main and auxiliary winding voltages and currents to the analyzer's four inputs. The analyzer was programmed as shown in Appendix C to compute the following quantities:

- Main Winding RMS Voltage
- Main Winding RMS Current
- Main Winding Average Power
- Auxiliary Winding RMS Voltage
- Auxiliary Winding RMS Current
- Auxiliary Winding Average Power
- Auxiliary Winding Voltage Phase
- Frequency

The mechanical quantities recorded were average torque and rotor speed. A stroboscope was used to determine the rotor speed and average torque was measured with a load cell mounted on the alternator, connected to a bridge amplifier and calibrated to read directly in N-m.

4.2 Sources of Error

4.2.1 Modelling Error

Numerous assumptions are made in the derivation of the model used to describe the motor under test. These assumptions include a linear magnetic circuit and a sinusoidal winding distribution. Experimental data presented in the following figures show that these assumptions could be expected to introduce significant error. Although the voltage supplied to the motor had very low harmonic content, the winding currents showed a high level of odd harmonics.

Figure 13 shows the main and auxiliary winding voltages with a vertical scale of 100 V/div for a load of approximately 0.5 N-m. The corresponding winding currents are shown in figure 14 with a vertical scale of 2 A/div. Third harmonics due to saturation effects are particularly evident in the auxiliary winding current. Saturation effects are also apparent in the main winding current although the rectangular shape is somewhat unexpected.

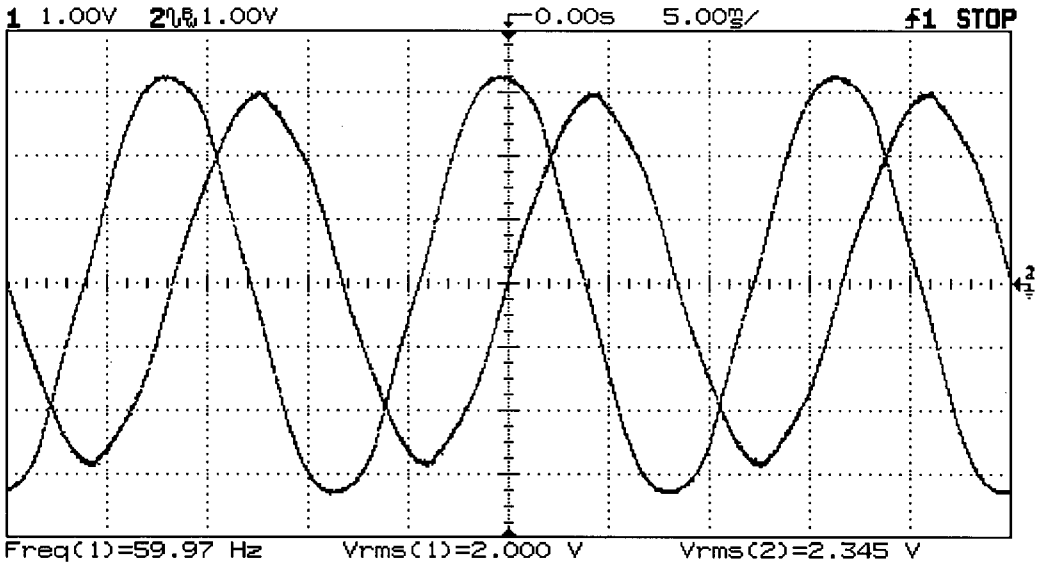

Figure 13: Main & Auxiliary Voltage

One unusual feature of the motor under test which may introduce additional error is the presence of a liquid filled stainless steel jacket between the rotor and stator. Although there is no experimental evidence in support of this claim, depending on the thickness of the jacket and the conductivity of the liquid, eddy current losses in the space between the rotor and stator could be rather

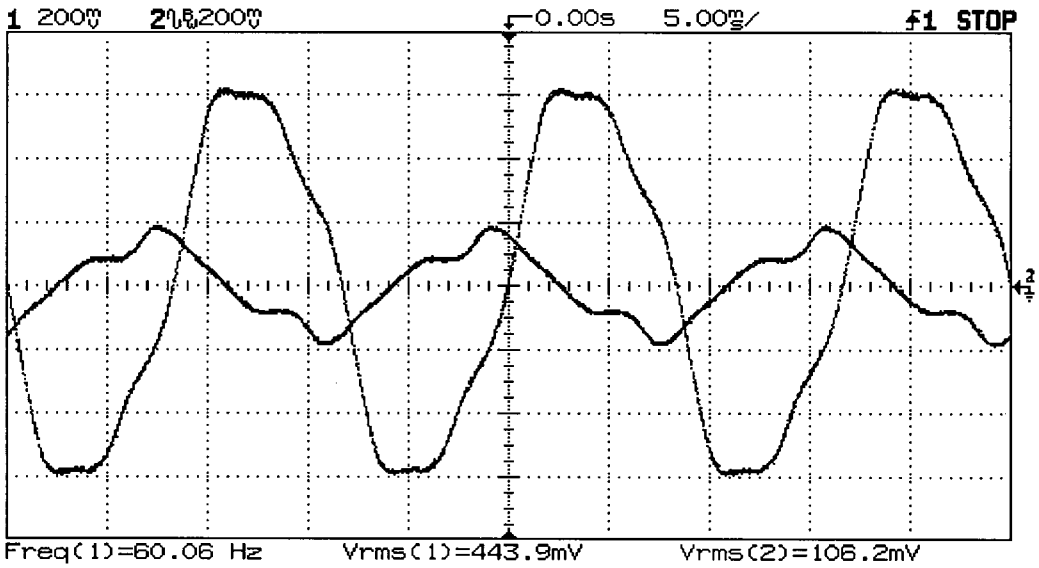

Figure 14: Main & Auxiliary Current

high. In conventional motors there are no conductive materials in this space, and consequently no eddy current losses.

4.2.2 Measurement Error

With the exception of the load cell, error introduced by instrumentation should be negligible. Voltages and currents measured by the isolation amplifiers and waveform analyzer compared well with values displayed by conventional metering. The largest source of measurement error is expected to be due to the load cell. Because the motor and alternator generated significant heat, the entire test fixture including the load cell was subjected to temperature cycling of up to 30°C during the course of experiments. Such large changes in the load cell temperature could be expected to introduce significant experimental error.

4.3 Efficiency Measurements

Figure 15 plots efficiency against auxiliary winding phase. The main winding voltage is supplied with 90% of rated voltage and the auxiliary winding voltage is set to 120% of the main winding voltage. Measurements at load torques of 0.5 N-m and 1.5 N-m correspond to 25% and 75% of rated torque respectively. The measured efficiencies compare quite well with simulation results and the maximum efficiency occurs when the auxiliary winding current leads the main winding current by slightly less than 90°. This result is predicted by the model as shown in figure 12.

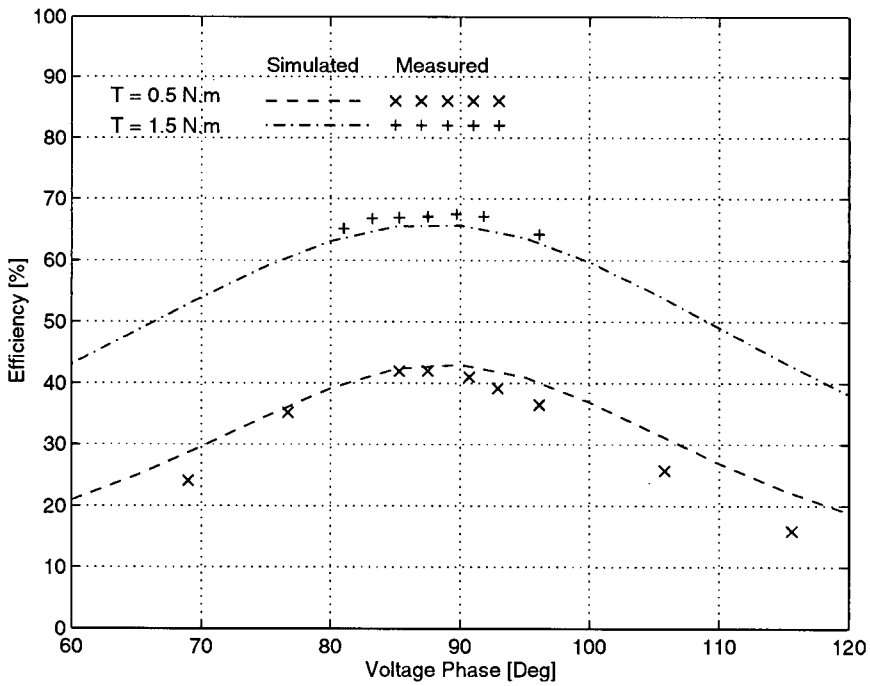

Figure 15: Dual Winding Efficiency vs. Auxiliary Voltage Phase Angle

Efficiency as a function of auxiliary winding voltage magnitude is shown in figure 16. The main winding voltage is fixed at 80% of rated voltage and the auxiliary winding voltage is varied between 90% and 130% of the main winding voltage. Auxiliary winding phase is fixed at 87.5°. Although the differences between measured and predicted efficiencies are slight and may be within experimental error the peak efficiencies occur at unexpected values of auxiliary winding voltage. Figure 11 shows that peak efficiency should be obtained when the auxiliary winding voltage is 120% of the main winding voltage. The data presented in figure 16 indicates that the optimum auxiliary winding voltage is between 105% and 115% of main winding voltage.

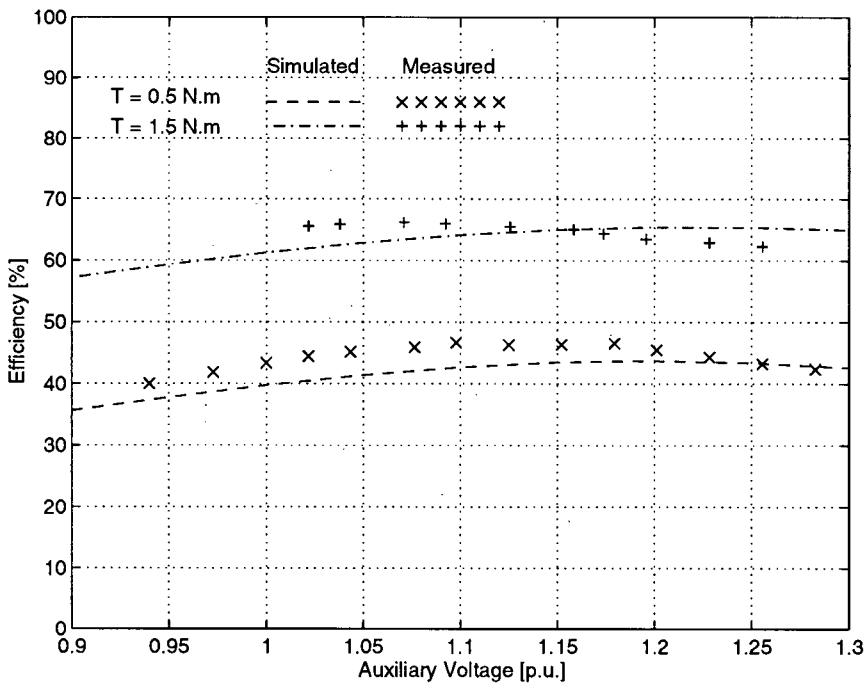

Figure 16: Dual Winding Efficiency vs. Auxiliary Voltage Magnitude

Figure 17 shows a plot of efficiency vs. main winding V/Hz ratio. For this experiment the auxiliary winding voltage was adjusted to 110% of the main winding voltage and the auxiliary winding phase was fixed at 87.5°. There are significant differences between measured and predicted efficiencies and at the two values of torque shown the peak efficiencies are higher than predicted by theory. In addition these peak efficiencies occur at lower V/Hz ratios than predicted by theory. This is most likely due to saturation effects which are not accounted for by the linear model used in the analysis.

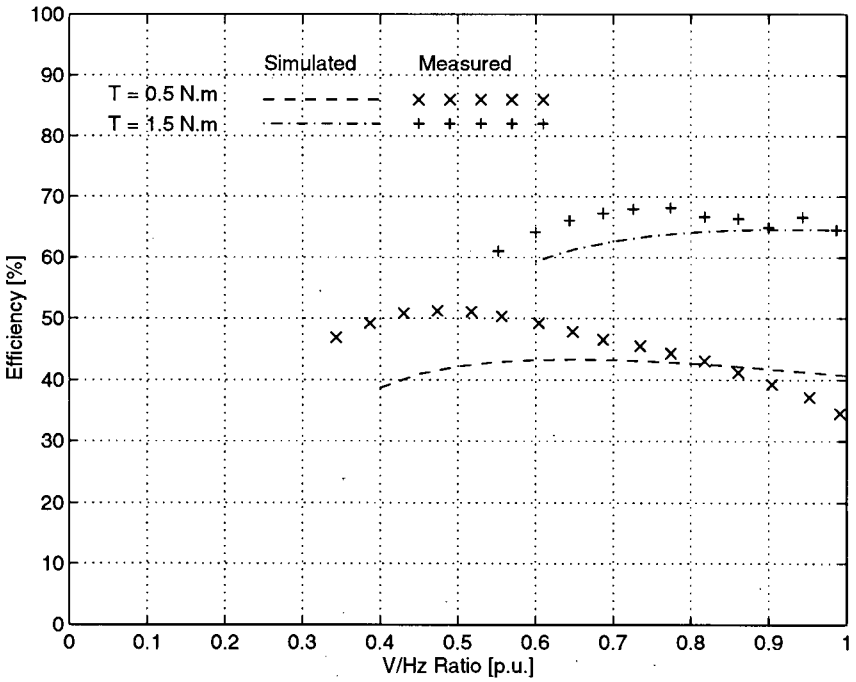

Figure 17: Dual Winding Efficiency vs. V/Hz Ratio

Other authors have reported efficiency improvements by operating at reduced

V/Hz ratios and thereby reducing core losses within the machine[6]. This particular machine is designed to be very compact and has a very small diameter in comparison to its length. Due to its compact design the machine could be expected to be well into saturation when operated at rated V/Hz.

To check this supposition similar tests were run with only the main winding of the machine excited and this data is presented in figure 18. Once again the effect of varying the V/Hz ratio is dramatic and peak efficiencies occur at lower V/Hz ratios than predicted by the model.

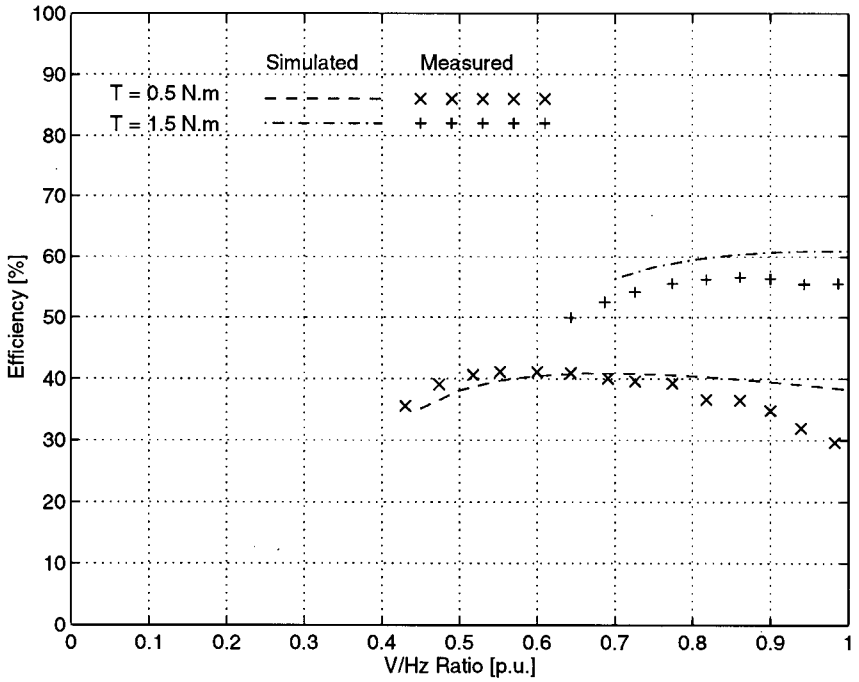

Figure 18: Single Winding Efficiency vs. V/Hz Ratio

By inspection of figures 17 and 18 it becomes clear that there is a relationship

between optimal V/Hz ratios and load torque for both single and dual winding excitation. Both figures show that at 25% of rated torque, efficiency is optimized when the V/Hz ratio is between 50% and 60% of rated value. At 75% of rated torque the optimum V/Hz ratio is between 75% and 85% of rated value. Based on these two data points, a linear approximation to the relationship can be written as:

$$\frac{V_m}{V_{rated}} = 0.4 + 0.5\frac{T_m}{T_{rated}} \tag{39}$$

Figure 19 compares measured efficiencies for single and dual winding excitation. In both cases the main winding voltage is adjusted according to equation 39. The upper data set represents auxiliary winding excitation at 110% of main winding voltage and a phase difference of 87.5°. There is clearly an efficiency improvement of approximately 5% and this improvement is consistent with that predicted by the model.

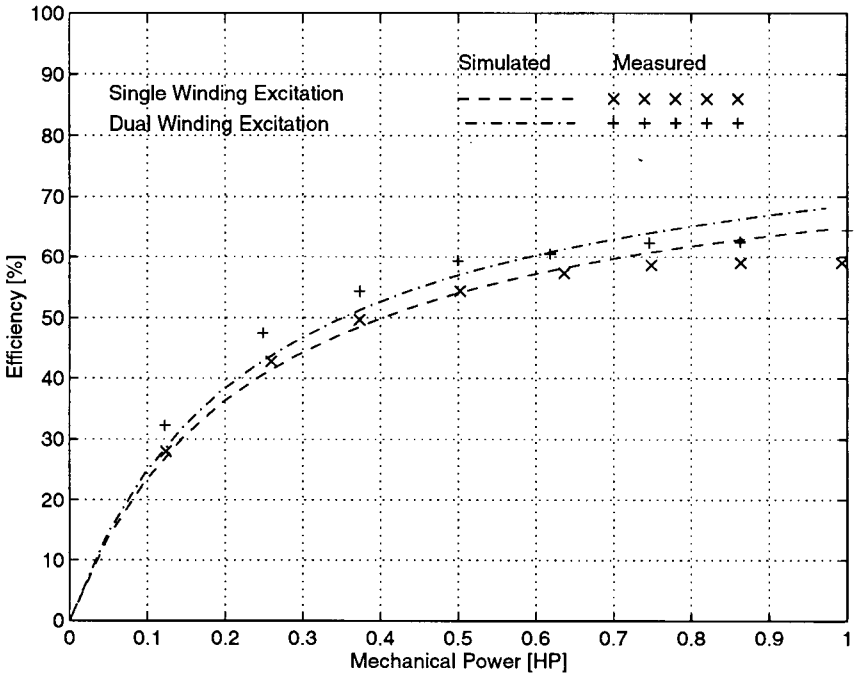

Figure 19: Efficiency vs. Mechanical Power

5 Conclusion

The objective of this analysis was to determine operating conditions which provide the highest possible efficiency for single-phase induction motors equipped with an auxiliary winding. The analysis was based on a model which is widely accepted and has been used by many authors[10, 13, 9, 12]. The computer simulations which have been presented confirm that the analysis correctly determines optimal operating conditions for motors which can be accurately described by the model.

Experimental measurements made with a submersible single-phase induction motor indicate that the effects predicted by theory are present and that it is possible to improve efficiency by excitation of the auxiliary winding. However, the peak efficiency does not occur under exactly the same conditions as predicted by theory and it appears that the linear model used for the analysis is not capable of accurately describing the motor under test. The model assumes that the permeability of the magnetic circuit is independent of flux density and that skin depth effects in both the rotor and stator are negligible. Depending on the type and construction of motor, both of these approximations could introduce significant error.

The highest accuracy could be expected for motors designed for high efficiency as these motors operate in the linear portion of the magnetization characteristic. On the other hand, the model could not be expected to accurately

predict the performance of compact motors designed for high starting torque. Increased starting torque is achieved by taking advantage of deep bar effects so that the rotor resistance is strongly dependent on slip frequency and is therefore very high during starting[12]. At constant slip, stator frequency and slip frequency are proportional and consequently rotor resistance increases with stator frequency. Compact motors typically have a smaller magnetic circuit cross section and so are further into saturation when operated at rated V/Hz.

The theory's ability to deal with modelling error could likely be improved by experimentally determining sets of parameters which depend on stator frequency and flux density. Provided voltage is adjusted in proportion to stator frequency, the flux density could be assumed constant and the dependence of model parameters on skin depth effects could be determined. The effects of changes in flux density could be determined by varying the V/Hz ratio at constant frequency. Although such an approach would limit the utility of the analytical work which has been presented here, if the equations were used in conjunction with computer simulations an accurate prediction of motor performance should be possible.

Despite the differences between experimental results and computer simulations the measured and predicted efficiency improvements compare quite closely. Experimental results presented in figure 18 show that, depending on operating point, considerable gains in efficiency are possible by operating with single winding excitation and properly choosing the V/Hz ratio to match the load. Because

of the ease with which this could be accomplished this should certainly be taken advantage of before resorting to dual winding excitation. For this particular motor, when operated at rated speed and 25% of rated torque, a 10% increase in efficiency was achieved by operating at approximately 60% of rated V/Hz. This optimal V/Hz ratio is consistent with that predicted by theory as shown in figure 10. Equation 39 can be used to approximate the optimal V/Hz ratio as a function of load torque.

In addition to what can be achieved by properly adjusting the V/Hz ratio, further efficiency improvements are possible by appropriate choices of auxiliary winding voltage magnitude and phase. Although it is the current phase which must be in quadrature to obtain peak efficiency, for all practical purposes it is sufficient to maintain the auxiliary winding voltage in quadrature with the main winding voltage.

For the motor under test, experimental results presented in figure 3 reveal that peak efficiency is obtained with the auxiliary winding voltage set to approximately 110% of the main winding voltage as shown in figure 15. When the machine is operated with these conditions on auxiliary voltage magnitude and phase, an additional 5% increase in efficiency is achieved at rated speed and over a wide range of load torques as shown in figure 19.

In a practical application this efficiency improvement would likely be offset by

losses within the auxiliary winding power conditioning unit and careful analysis would be required to determine if there would be any benefit to retrofitting such a power converter. The author therefore recommends that any project undertaken to improve the efficiency of systems using solar powered inverter driven submersible single-phase motors such as the Franklin Electric model 2143084416 be completed in two stages.

The first stage should be to experimentally determine optimal V/Hz ratios for single winding excitation under a number of operating conditions. These ratios should then be correlated to rotor speed and torque and the inverter software should be modified to adjust the modulation index depending on operating point. Stator frequency and winding current should be sufficient to determine operating point as these quantities are very closely related to rotor speed and torque. This solution would not involve any hardware changes to existing systems and would therefore be a very inexpensive means of improving efficiency.

If additional improvements are desired after modifying the system to operate at optimal V/Hz ratios, the first step should be an economic analysis. Because the potential gain in efficiency is quite small, the cost of an auxiliary winding power converter may not be justified by the savings in solar cells. In this instance, the motor under test is rated at one horsepower and at rated load reaches its peak efficiency of approximately 65%. At rated load an increase in efficiency of 5% would therefore reduce the electrical input power by 82 Watts. Assuming that

the solar cells can be obtained at a cost of $5 per Watt, potential savings would be $410 less the cost of additional power electronics required for the auxiliary winding power converter. If such savings are large enough to be of interest the proposed implementation described in Appendix B could be applied.

Appendix A
Equivalent Circuit Parameters

The method suggested by Veinott[13] is used to compute equivalent circuit parameters based on DC winding resistance, locked-rotor and no-load tests. The usual approximations made in order to obtain equivalent circuit parameters from these tests neglect the effects of magnetizing reactance on the locked-rotor impedance. It is claimed that Veinott's method provides improved accuracy by introducing a slight modification to account for these effects.

This method does not provide all of the parameters required to model a single-phase induction motor with both main and auxiliary windings. The two additional required parameters model the auxiliary winding stator leakage reactance and the effective turns ratio between main and auxiliary windings. The manufacturer was able to provide the turns ratio and the leakage reactance was approximated from locked-rotor measurements, turns ratio and rotor leakage reactance.

f_s [Hz]	V_{Lm} [V]	I_{Lm} [A]	P_{Lm} [W]	V_{La} [V]	I_{La} [A]	P_{La} [W]
30	27.3	5.00	114	39.2	2.50	91
40	30.5	5.02	117	41.1	2.47	87
50	33.6	5.01	121	44.0	2.53	96
60	37.3	5.04	124	45.9	2.49	91

Table 2: Locked-Rotor Measurements

f_s [Hz]	V_o [V]	I_o [A]	P_o [W]	ω_m [RPM]
30	104	4.61	165	1790
40	138	4.63	215	2392
50	173	4.68	265	2990
60	206	4.73	335	3590

Table 3: No-load Measurements

During no-load measurements both line current and input power increased sharply as the rated V/Hz ratio was approached. This effect is to be expected and is due to saturation of the magnetic circuit. While efficient operation at higher than rated V/Hz is not possible, it was expected that reducing the V/Hz ratio could improve efficiency. No-load measurements were therefore made at 90% of rated V/Hz in order to obtain a linearized model which could more accurately predict performance over the anticipated range of V/Hz ratios.

The equations which must be applied to the locked-rotor and no-load data are[13]:

$$P = \frac{W_{Lm}}{I_{Lm}^2} - r_1 \tag{40}$$

$$Q = \sqrt{\left(\frac{V_{Lm}}{I_{Lm}}\right)^2 - \left(\frac{W_{Lm}}{I_{Lm}^2}\right)^2} \tag{41}$$

$$X = x_1 + x_2 = \frac{V_o}{I_o} - \sqrt{\left(\frac{V_o}{I_o} - Q\right)^2 + P^2} \tag{42}$$

$$X_o = x_1 + x_m = \frac{2V_o}{I_o} - X \tag{43}$$

f_s $[Hz]$	r_1 $[\Omega]$	$\frac{x_1}{\omega_s}$ $[mH]$	r_{1a} $[\Omega]$	$\frac{x_{1a}}{\omega_s}$ $[mH]$	r_2 $[\Omega]$	$\frac{x_2}{\omega_s}$ $[mH]$	a $[p.u.]$
30	2.63	7.9	11.9	18.9	2.08	7.9	1.234
40	2.63	7.8	11.9	22.3	2.16	7.8	1.234
50	2.63	7.4	11.9	16.7	2.35	7.4	1.234
60	2.63	7.4	11.9	18.3	2.42	7.4	1.234

Table 4: Equivalent Circuit Parameters

In a squirrel-cage single-phase induction motor there is no way to separate rotor and stator leakage reactances and it is common practice to assume them to be equal[13, 9]. Under this assumption equations 42 and 43 can be solved to yield:

$$x_1 = x_2 = X_o\left(1 - \sqrt{1 - X/X_o}\right) \tag{44}$$

and:

$$x_m = X_o - x_1 \tag{45}$$

The auxiliary winding leakage reactance is approximated by neglecting the effects of magnetizing reactance and computing the input reactance from the auxiliary winding locked-rotor measurements. This input reactance is the sum of rotor and stator leakage reactances. Because the rotor leakage reactance is specified with respect to the main winding it must be referred to the auxiliary winding by the turns ratio. The auxiliary winding stator leakage reactance is approximated by[13]:

$$x_{1a} \approx \sqrt{\left(\frac{V_{La}}{I_{La}}\right)^2 - \left(\frac{W_{La}}{I_{La}^2}\right)^2} - a^2 x_2 \tag{46}$$

These parameters determine the electrical characteristics of a single-phase induction motor but can not model the effects of friction and windage on the mechanical performance. Friction and windage losses can be approximated from the no-load measurements and equivalent circuit parameters. This is done by assuming that friction and windage losses are given by the difference between measured input power and resistive losses as computed from equivalent circuit parameters and measured current.

$$P_{fw} = P_o - (r_1 + R_f + R_b)I_o^2 \approx B\omega_m^n \tag{47}$$

Regression analysis on experimental data reveals that the appropriate values of the required constants are:

$$\begin{aligned} B &= 0.24 \\ n &= 1.12 \end{aligned} \tag{48}$$

when w_m is specified in rad/s. This data is presented in figure 20.

The manufacturer of the motor was able to provide a plot of experimentally determined performance characteristics and this is displayed in figure 21. This data is used as a benchmark to determine the validity of the equivalent circuit model as well as the parameters used in the model. Figure 22 shows the results of a computer simulation run under the same conditions as the experimental measurements. The agreement between the two sets of data is quite good, indicating that the model and parameter set accurately describe motor performance.

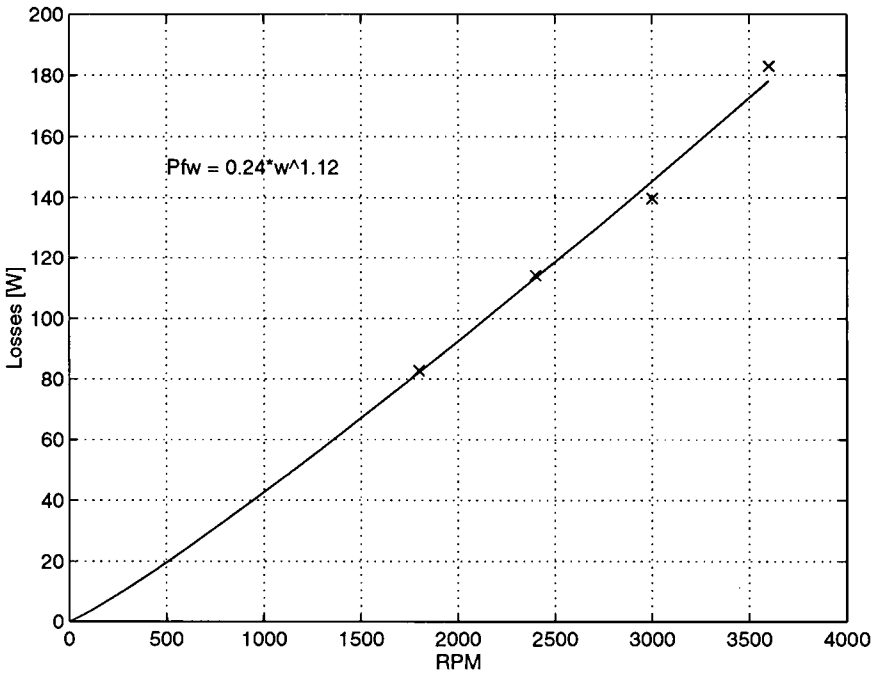

Figure 20: Friction and Windage Losses vs. Rotor Speed

Franklin Electric

MOTOR PERFORMANCE CHARACTERISTICS

TEST				
	VOLTS	230	HERTZ	60
	ST. MFD	116.6	RUN MFD	
	TEST PR	2647	PAGE	119
	APPR BY		DATE	7-14-92

RATING				
	FRAME	4 INCH SUB	HP	1
	MODEL	2143081216	VOLTS	230
	RPM	3450	PHASE	1
	S.F.	1.4	HERTZ	60
	TYPE	CSIR		

REMARKS: TESTED IN WATER, SHAFT UP, WITH NO APPLIED THRUST.
CALIBRATED MOTOR.
TEST ON ONE MOTOR. NOT GUARANTEED AS MINIMUM PERFORMANCE.

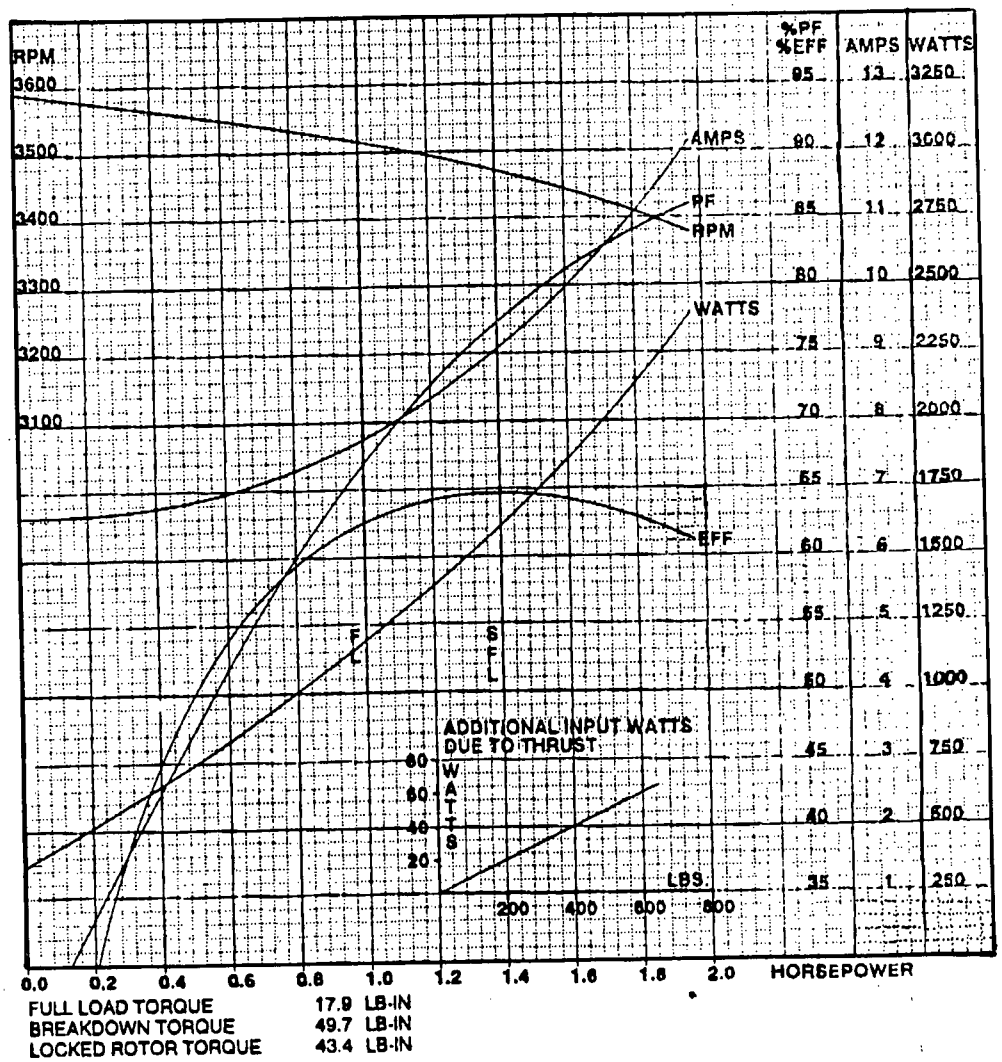

FULL LOAD TORQUE	17.9	LB-IN
BREAKDOWN TORQUE	49.7	LB-IN
LOCKED ROTOR TORQUE	43.4	LB-IN

Figure 21: Measured Motor Characteristics

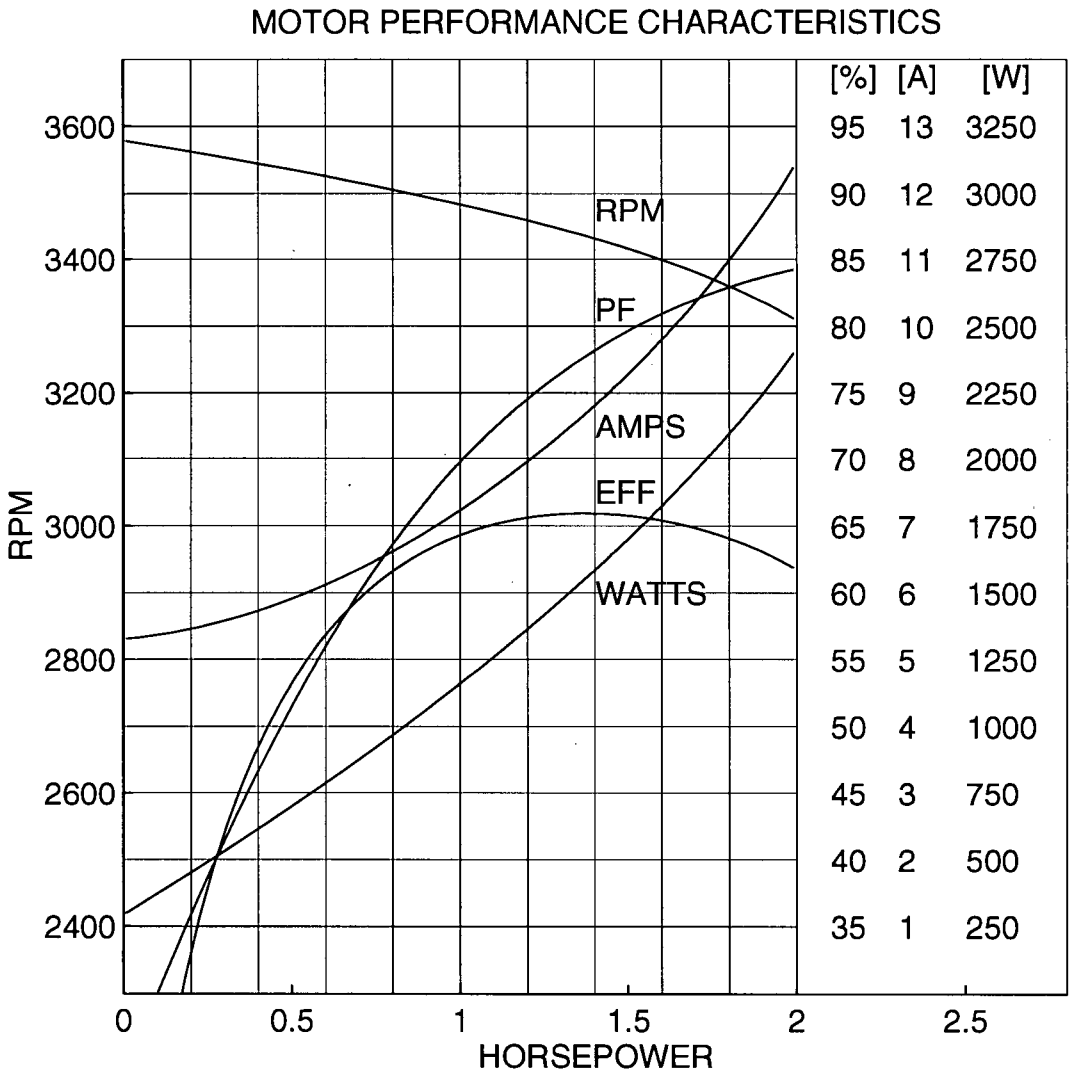

Figure 22: Simulated Motor Characteristics

Appendix B
Proposed Implementation

When used for photo-voltaic pumping applications, the single-phase induction motor studied here is commonly powered by a single phase inverter. Because the voltage provided by the solar cells is relatively low, the inverter is usually an H-bridge with trapezoidal or sine-coded pulse width modulation. If sine-coded modulation is used, a third harmonic component is sometimes added to increase the magnitude of the fundamental component.

Some changes to this approach will be required in order to supply the auxiliary winding. One option would be to provide a second H-bridge for the auxiliary winding. However, because the main and auxiliary windings share a common neutral, the auxiliary inverter would have to be isolated from the main inverter and the cost of providing this isolation is likely to be prohibitive. Without isolation, a three phase inverter is the only practical way to provide the required phase difference between main and auxiliary windings.

As shown in figure 23 the auxiliary winding voltage which can be provided is limited by the required main winding voltage and the relative phase. The maximum fundamental phase voltage which can be provided by a single leg of a sine-coded PWM inverter is given by:

$$V_{ph} = \frac{V_{dc}}{2\sqrt{2}} \tag{49}$$

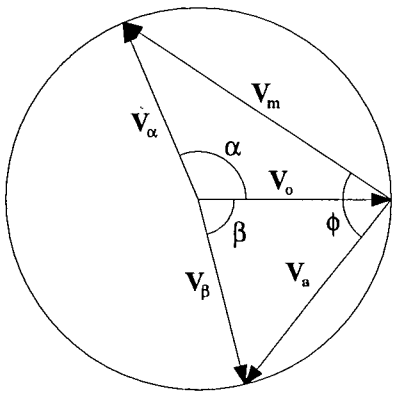

Figure 23: Voltage Utilization of Three Phase Inverter

With this limitation on phase voltage, the main and auxiliary winding voltages are limited to:

$$\begin{aligned} V_m &= \frac{V_{dc}}{2}\sqrt{1-\cos\alpha} \\ V_a &= \frac{V_{dc}}{2}\sqrt{1-\cos\beta} \end{aligned} \tag{50}$$

The phase displacement required to generate the desired main winding voltage is given by:

$$\alpha = \cos^{-1}\left(1 - 4\frac{V_m^2}{V_{dc}^2}\right) \tag{51}$$

Because the relative phase between main and auxiliary winding voltages can be written as:

$$\phi = \pi - \frac{\alpha+\beta}{2} \tag{52}$$

the phase displacement required for the auxiliary winding phase is given by:

$$\beta = 2(\pi-\phi) - \alpha = 2(\pi-\phi) - \cos^{-1}\left(1 - 4\frac{V_m^2}{V_{dc}^2}\right) \tag{53}$$

The maximum available auxiliary winding voltage, as a function of main winding voltage and relative phase, is therefore:

$$V_a = \frac{V_{dc}}{2}\sqrt{1 - \cos\left[2\phi + \cos^{-1}\left(1 - 4\frac{V_m^2}{V_{dc}^2}\right)\right]} \tag{54}$$

When the main and auxiliary winding voltages are in quadrature $\phi = \pi/2$ and this relationship simplifies to the Pythagorean Theorem.

$$V_m^2 + V_a^2 = \frac{V_{dc}^2}{2} = \left(2V_{ph}^2\right) \tag{55}$$

As the main winding voltage approaches $\sqrt{2}V_{ph}$ the voltage available for the auxiliary winding phase is very low. For the motor under test the power factor at rated load is approximately 70% as shown in figure 21. The winding currents therefore lag terminal voltages by approximately 45° and a portion of the auxiliary winding phase shift could be provided by a series capacitor as shown in figure 24.

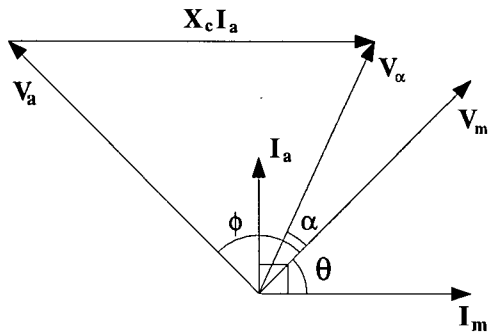

Figure 24: Auxiliary Winding Compensation

For this application the optimum compensating reactance can be defined as the value which minimizes the required link voltage over the desired range of

speeds and torques. The optimum slip is independent of torque but varies with rotor speed as shown in figures 4 and 6 respectively. Consequently the impedance matrix, which has slip dependent terms which are presented in equation 1, depends only on rotor speed. As a result the choice of compensating reactance is also independent of torque.

It is possible to show that for a compensating reactance X_c the quantities V_α and α in figure 24 are given by:

$$V_\alpha = \sqrt{[X_c I_a + V_a \cos(\theta + \phi)]^2 + [V_a \sin(\theta + \phi)]^2} \tag{56}$$

and:

$$\alpha = \cos^{-1}\left(\frac{X_c I_a + V_a \cos(\theta + \phi)}{V_\alpha}\right) - \theta \tag{57}$$

The required link voltage V_{dc} can therefore determined by solving:

$$V_\alpha = \frac{V_{dc}}{2}\sqrt{1 - \cos\left[2\alpha + \cos^{-1}\left(1 - 4\frac{V_m^2}{V_{dc}^2}\right)\right]} \tag{58}$$

Given that:

$$\cos\left(\gamma + \cos^{-1} X\right) = X\cos\gamma - \sqrt{1 - X^2}\sin\gamma \tag{59}$$

equation 58 can be rewritten as a quadratic in V_{dc}^2:

$$A\left(V_{dc}^2\right)^2 + B\left(V_{dc}^2\right) + C = 0 \tag{60}$$

where:

$$\begin{aligned} A &= [1 - \cos(2\alpha)]^2 \\ B &= -[1 - \cos(2\alpha)]\left[(2V_m)^2 + (2V_\alpha)^2\right] \\ C &= (2V_m)^4 - 2(2V_m)^2(2V_\alpha)^2\cos(2\alpha) + (2V_\alpha)^4 \end{aligned} \tag{61}$$

The required link voltage can therefore be determined by applying the quadratic formula to equation 60. When rated voltage is applied to the main winding, and the auxiliary winding voltage magnitude and phase are chosen to provide optimum performance, the link voltage is as shown in figure 25. There are two capacitances which result in the same minimum link voltage. Although the smaller capacitor would be less expensive, the link voltage increases abruptly for small deviations from this optimum value. Consequently the larger value would be a more practical choice.

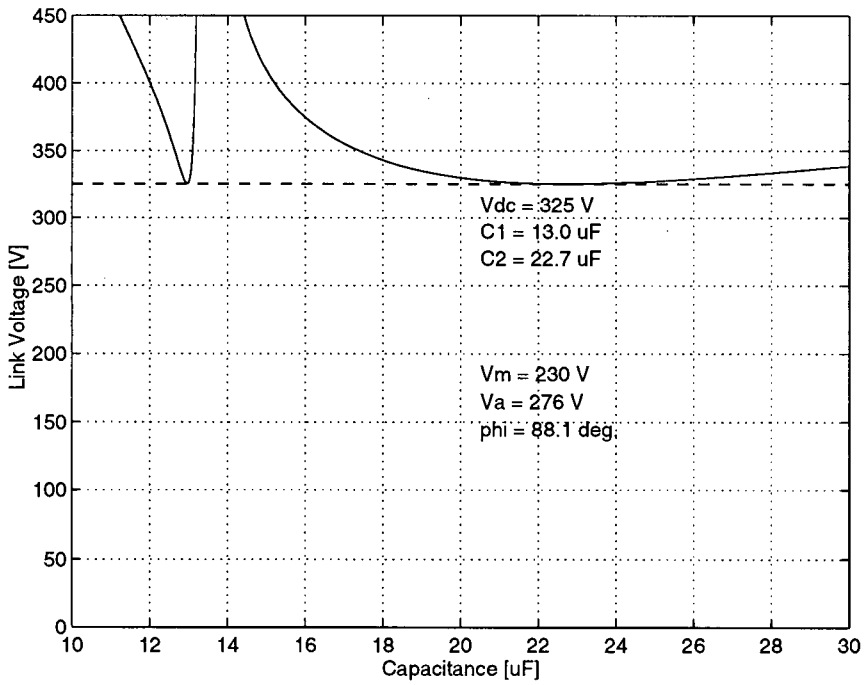

Figure 25: Link Voltage vs. Run Capacitance

The values shown in figure 25 are only optimal at rated stator frequency but the approach could be extended to determine a single value of capacitance which minimizes link voltage over the range of anticipated stator frequencies.

Appendix C
Waveform Analyzer Program

This program is written for the Data Precision model Data 6000A waveform analyzer. Input buffers are sampled in lines 10 through 40. Instantaneous power is computed as a point by point multiplication of voltage and current for the main and auxiliary windings in lines 50 and 60 respectively. Cursor positions for positive zero crossings of the main and auxiliary winding voltages are measured in lines 70 and 80 and this information is used in lines 100 through 120 to compute the phase of the auxiliary winding voltage relative to that of the main winding.

```
10  VM = UNIT(BUF.A1,2,0,100,2)
20  IM = UNIT(BUF.A2,2,0,10,48)
30  VA = UNIT(BUF.A3,2,0,100,2)
40  IA = UNIT(BUF.A4,2,0,10,48)
50  PM = VM*IM
60  PA = VA*IA
70  DSPL(SC:CRSP(BUF.A3))
80  DSPL(NX:SE:CRSP(BUF.A1))
90  F = FREQ(VM)
100 PHI = 360*XDELTA*F
110 PHI = PHI-180
120 PHI = UNIT(PHI,2,0,1,41)
130 DSPL(F)
140 DSPL(PHI)
150 DSPL(RMS(VM))
160 DSPL(RMS(IM))
170 DSPL(MEAN(PM))
180 DSPL(RMS(VA))
190 DSPL(RMS(IA))
200 DSPL(MEAN(PA))
```

References

[1] Bernard Adkins. *The General Theory of Electrical Machines*. Chapman & Hall, London, 1957.

[2] Philip L. Alger. *Induction Machines: Their Behaviour and Uses, 2nd Ed.* Gordon and Breach Scientific Publishers, New York, 1970.

[3] A. Vandenput et al. Run capacitor optimization in single-phase induction motors. *IEEE Industrial Applications Conference Proceedings*, 1986.

[4] E. R. Collins Jr. et al. Single-phase induction motor adjustable speed drive: Direct phase angle control of the auxiliary winding supply. *IEEE Trans. on Industrial Applications, Vol. 35, No. 6, pp. 246–252*, 1988.

[5] H. Huang, E.F. Fuchs, and J.C. White. Optimal placement of the run capacitor in single-phase induction motor designs. *IEEE Trans. on Energy Conversion, Vol. EC-3, No. 3, pp. 647–652*, September, 1988.

[6] Joseph D. Law and Thomas A. Lipo. A single phase induction motor voltage controller with improved performance. *IEEE Trans. on Power Electronics, Vol. PE-1, No. 4, pp. 240–247*, October, 1986.

[7] Terrance M. Lettenmaier, Donald W. Novotny, and Thomas A. Lipo. Single phase induction motor with electronically controlled capacitor. *IEEE Trans. on Industrial Applications, Vol. 35, No. 6, pp. 169–174*, 1988.

[8] Jerrold E. Marsden and Anthony Tromba. *Vector Calculus*. W. H. Freeman, 1981.

[9] Leander W. Matsch and J. Derald Morgan. *Electromagnetic and Electromechanical Machines, 3rd Ed.* John Wiley & Sons, Toronto, 1986.

[10] Wayne J. Morrill. The revolving field theory of the capacitor motor. *Trans. AIEE, Vol. 48, pp. 614–629*, April, 1929.

[11] J.M.D. Murphy and F.G. Turnbull. *Power Electronic Control of AC Motors.* Pergamon Press, Toronto, 1989.

[12] Gordon R. Slemon and A. Straughen. *Electric Machines.* Addison-Wesley, 1980.

[13] Cyril G. Veinott. *Theory and Design of Small Induction Motors.* McGraw-Hill, New York, 1959.

[14] Herbert Vickers. *The Induction Motor, 2nd Ed.* Sir Isaac Pitman & Sons, London, 1953.